Single-cell spatial mapping reveals alteration of cell type composition and tissue microenvironment during early colorectal cancer formation

Tuhin K. Guha[1], Edward D. Esplin[1], Aaron M. Horning[2], Roxanne Chiu[3], Kristina Paul[1], Annika K. Weimer [1,4], Winston R. Becker[5], Rozelle Laquindanum[6], Meredith A. Mills[6], D. Glen Esplin[7], Jeanne Shen[8], Emma Monte[1], Shannon White[1], Thomas V. Karathanos[1], Daniel Cotter[1], Joanna Bi[1], Uri Ladabaum[6], Teri A. Longacre[8], Christina Curtis[1,6], William J. Greenleaf[1,9], James M. Ford[1,6#], Michael P. Snyder[1#]

1 Department of Genetics, Stanford School of Medicine, Stanford, CA 94305
2 Amgen, South San Francisco, CA 94080
3 Guardant Health, Redwood City, CA 94063
4 Novo Nordisk Foundation Center for Genomic Mechanisms of Disease, Broad Institute of MIT and Harvard, Cambridge, MA 02142, USA
5 Dana-Farber Cancer Institute, Boston, MA 02215
6 Department of Medicine, Stanford School of Medicine, Stanford, CA 94305
7 Animal Reference Pathology, Salt Lake City, UT 84107
8 Department of Pathology, Stanford School of Medicine, Stanford, CA 94305
9 Chan Zuckerberg Biohub, San Francisco, CA, USA

co-corresponding authors

Abstract

Colorectal cancer (CRC) is the third leading cause of cancer mortality in the United States. Familial adenomatous polyposis (FAP) is a hereditary syndrome that raises the risk of developing CRC, with total colectomy as the only effective prevention. Even though FAP is rare (0.5% of all CRC cases), this disease model is well suited for studying the early stages of malignant transformation as patients form many polyps reflective of pre-cancer states. In order to spatially profile and analyze the pre-cancer and tumor microenvironment, we have performed single-cell multiplexed imaging for 52 samples: 12 normal mucosa,16 FAP mucosa,18 FAP polyps, 2 FAP adenocarcinoma, and 4 sporadic colorectal cancer (CRCs) using Co-detection by Indexing (CODEX) imaging platform. The data revealed significant changes in cell type composition occurring in early stage polyps and during the malignant transformation of polyps to CRC. We observe a decrease in CD4+/CD8+ T cell ratio and M1/M2 macrophage ratio along the FAP disease continuum. Advanced dysplastic polyps show a higher population of cancer associated fibroblasts (CAFs), which likely alter the pre-cancer microenvironment. Within polyps and CRCs, we observe strong nuclear expression of beta-catenin and higher number neo-angiogenesis events, unlike FAP mucosa and normal colon counterparts. We identify an increase in cancer stem cells (CSCs) within the glandular crypts of the FAP polyps and also detect Tregs, tumor associated macrophages (TAMs) and vascular endothelial cells supporting CSC survival and proliferation. We detect a potential immunosuppressive microenvironment within the tumor 'nest' of FAP adenocarcinoma samples, where tumor cells tend to segregate and remain distant from the invading immune cells. TAMs were found to infiltrate the tumor area, along with angiogenesis and tumor proliferation. CAFs were found to be enriched near the inflammatory region within polyps and CRCs and may have several roles in supporting tumor growth. Neighborhood analyses between adjacent FAP mucosa and FAP polyps show significant differences in spatial location of cells based on functionality. For example, in FAP

mucosa, naive CD4+ T cells alone tend to localize near the fibroblast within the stromal compartment. However, in FAP polyp, CD4+T cells colocalize with the macrophages for T cell activation. Our data are expected to serve as a useful resource for understanding the early stages of neogenesis and the pre-cancer microenvironment, which may benefit early detection, therapeutic intervention and future prevention.

Keywords: Familial adenomatous polyposis (FAP), colorectal cancer, pre-cancer microenvironment, Co-detection by Indexing (CODEX), cell type composition, neighborhood analysis

Introduction

Oncogenesis involves a complex series of events that occur during neogenesis to premalignant states to malignant tumors[1,2]. There are many genomic events that occur during this process, but most of the complex molecular interactions remain largely unknown during the early stages of cancer initiation, commonly known as pre-cancer[3,4].

Colorectal adenocarcinoma (CRC) is the third leading cause of cancer mortality in the U.S[7] and colorectal adenocarcinoma (CRC) is an excellent model to investigate pre-cancer events. Early stage polyps can be observed and isolated, and phenotypes associated with malignant transformation can be followed[5,6]. More than 90% of all CRC patients possess mutations that affect the Wnt signaling pathway, with more than 80% of these containing mutations in the Wnt-antagonist Adenomatous polyposis colitis (APC) gene. It is now well established that the APC protein acts as a scaffold in the β-catenin destruction complex thereby regulating the Wnt signaling pathway, which otherwise leads to intestinal hyperplasia[8-10]. APC mutations are thought to initiate events of colorectal carcinogenesis and are the major cause of the hereditary colon cancer syndrome known as Familial Adenomatous Polyposis (FAP). In patients with FAP, the number of polyps that develop by the time of early adulthood is typically 100 or more[11,12]. Thus, a single patient may present multiple polyps of varying molecular ages and stages of development, all of which are derived from a common germ lineage[13-15]. The majority of research on advanced-stage tumors has been limited to bulk profiling and has largely disregarded premalignant lesions (pre-cancer events). Therefore, the full phenotypic alteration that occurs in the transition from baseline mucosa to pre-cancerous polyp to malignant status remains to be fully elucidated.

Previous studies have mapped cell types in sporadic polyps and those of FAP patients using single-cell RNA-sequencing (scRNA-seq), assay for transposase-accessible chromatin with sequencing (ATAC-seq) and have detected cell types and transcriptional regulation programs within these polyps[16,17]. However, the differences with regard to the cellular spatial context, composition of the functional neighborhoods, as well as the molecular changes within the tissue microenvironment (TME) of this disease continuum from healthy colon to invasive adenocarcinoma is not well characterized. In order to understand the differences within TMEs during FAP disease progression, and as a part of the Human Tumor Atlas Network (HTAN)[18], we extend our previous research[17] by spatially mapping single cells from premalignant polyps, CRCs and normal mucosa (healthy controls) using C-Detection by indEXing (CODEX) single-cell multiplexed imaging platform[19,20].

Pretumorigenic activity within polyps is likely to be mediated by the effects on DNA damage response and immune signaling, as well as other mechanisms such as changes in cell type composition, that may be exacerbated during the course of disease progression[16]. Through spatial profiling we investigate the cell composition and organization in normal, polyps of different stages and adenocarcinomas.

We observe an increase in stem-like cells, endothelial cells, cancer-associated fibroblasts (CAFs), regulatory T cells (Tregs), and M2 macrophages during the FAP disease progression, thereby providing a suitable pre-cancer microenvironment for tumor cells to proliferate. In contrast, enterocytes, goblet cells, cycling Transit Amplifying (TA) , and natural-killer cells (NK) decrease along the disease continuum. When compared to normal and FAP mucosa, we find two critical determinants of disease prognosis, such as CD4+:CD8+ T cell ratio and M1:M2 macrophage ratio decrease in FAP polyp and adenocarcinoma/sporadic CRC samples. Compared to their counterparts in the FAP mucosa and normal colon, polyps and CRCs exhibit higher neo-angiogenesis events and strong nuclear expression of beta-catenin. Within the glandular crypts of the FAP polyps, we find an increase in cancer stem cells (CSCs). Additionally, we find Tregs, tumor associated macrophages (TAMs), and vascular endothelial cells that potentially promote the survival and proliferation of CSCs. In the tumor "nest" of FAP adenocarcinoma samples, we find an immunosuppressive microenvironment where tumor cells are spatially separated from the immune cells. Additionally, it has been observed that TAMs penetrate the tumorous region, promoting angiogenesis and tumor growth. We find that CAFs play a number of roles in supporting tumor growth and are typically found close to the inflammatory region within polyps and CRCs. Through neighborhood analyses, we also find distinct cell-cell localization relevant to various FAP disease states and also show differences in cell type location between adjacent FAP mucosa and FAP polyps based on biological functionality. Understanding the cellular and molecular dynamics through single-cell spatial biology during early colorectal tumorigenesis will not only provide insights into mechanisms of CRC progression and prevention, valuable to scientific research communities but will also add another dimension to single-cell analysis by understanding how cells organize and interact across the pre-cancer landscape required for disease progression, response to therapy, and potential preventive intervention.

Results

CODEX generates single-cell spatial maps from FAP and non-FAP donor tissue samples

We generated CODEX single-cell spatial data from 52 samples [12 normal mucosa, 16 FAP mucosa, 18 FAP polyps, 2 FAP adenocarcinoma and, 4 sporadic colorectal cancer (CRCs)] collected across 11 FAP-affected individuals and 8 non-FAP individuals (**Fig.1a)** Out of 19 donors, there were 12 males and 8 females: 9 Hispanic individuals, 10 European individuals and 1 Black individual. Age ranges were from 12 to 78 years (**Supplementary Table 1**). Different collection methods such as colectomy, colonoscopy and pouchoscopy were used to procure tissue samples. CODEX was performed on tissue samples collected from ascending, transverse, descending, and sigmoid regions of the both FAP affected and normal mucosa. **(Supplementary Table 2**).

The CODEX instrument (Akoya Biosciences) stains a tissue section with up to 42 oligo-conjugated antibodies probed against different protein targets within the tissue **(Supplementary Fig. 1).** This single-cell imaging modality is particularly helpful in providing cell composition and spatial relationship of cell types within multicellular tissue, thereby proving valuable insights into cell-cell interactions with possible biological significance. The majority of the cell type markers selected for CODEX imaging were based on our previous findings, where single-nuclei RNA (snRNA) and single-nuclei Assay for Transposase-Accessible Chromatin with high-throughput sequencing (snATAC) revealed cell-specific marker information[17]. Forty-two antibodies representing different cell types were selected and validated for specificity using protocols optimized for fresh frozen samples (see methods; **Supplementary Fig. 2**). This antibody marker panel **(Supplementary Table 3)** was used to stain the tissue, polyp and tumor samples from

normal mucosa, FAP mucosa, FAP polyp and adenocarcinoma/CRC respectively (**Fig.1b)**, thereby enabling spatial detection and distribution of up to 25 cell types across the FAP disease continuum.

CODEX imaging shows changes in cell type composition across malignant transformation

We generated 52 CODEX tissue images, which were processed, segmented and annotated for cell type identification using the antibody/marker-based approach[20]. The resultant dataset was used to observe the overall tissue morphology **(Supplementary Fig. 3)** and quantify and compare the cell type composition between the normal mucosa and the FAP disease states. Overall, across the different disease states (normal, FAP mucosa, benign polyps, dysplastic polyps, adenocarcinoma) we observed an increase in stem-like cells, endothelial cells, cancer-associated fibroblasts (CAFs), CD8+ T cells, regulatory T cells (Tregs), exhausted T cells (present only in adenocarcinoma/sporadic CRC), and M2 macrophages and decrease in enterocytes, goblet cells, transit-amplifying cells (TA), cycling TA cells, CD4+ T cells, NK cells and neuroendocrine cells (**Fig. 1b, c**). However, certain cell types such as smooth muscle, nerve, lymphatic endothelial, and enteroendocrine remained relatively stable across disease states (**Fig.1,b, c)**. We find that the percentage of stem-like cell populations within the crypts of normal mucosa decreases with the increase in age of the healthy donors (Pearson coefficient r = 0.9). However, in FAP mucosa we observe both an increase in stem-like cells, and decreased correlation between the fraction of stem-like cells and the age of FAP patients (Pearson coefficient r = 0.2). For example, in one case a 62-year-old FAP patient had a similar fraction of stem-like cells to a 38-year-old patient (**Fig.1d)**. Polyps collected from a 26-year-old and a 54-year-old FAP patient show similar immune cell type composition within the sub-mucosal intestinal lymphoid follicles (sm-ILF). For both cases, we observe dendritic cells (DC), CD4+ and CD8+ double positive T cells, PD1 marker expression within the germinal centers and vascular cells at the follicular periphery. Moreover, we observe a higher number of DC and a lower number of B cells within solitary intestinal lymphoid follicles (SILT) compared to that within sm-ILF from the same polyp sample collected from the 54-year-old patient. **(Supplementary Fig. 4)**.

The CD4+/CD8+ T cell ratio is associated with colorectal cancer prognosis[22,23]. Increased immune function is strongly correlated with higher CD4+/CD8+ T cell ratio[24,25]. We observe that the overall ratio of CD4+/ CD8+ T cells was significantly higher in normal mucosa and decreased along the FAP disease continuum (**Fig.1e)**. We also observe the spatial distribution of CD4+ T cells and CD8+ T cells within the pre-cancer microenvironment, where higher number of CD4+ T cells tend to localize in the stromal compartment within the FAP mucosa. In contrast, the FAP polyps exhibit a relatively higher number of CD8+ T cells than CD4+ T cells and the former happens to be in direct contact with the intestinal epithelial cells (IECs) (**Fig.1f)**.

Goblet cells secrete a protective mucus gel composed predominantly of mucin glyco-proteins that protects the gastrointestinal epithelial layer[27-29]. While analyzing the overall goblet cell composition between both the sexes, we found that the percentage of mucin producing cells tends to be higher in females compared to male patients (**Fig.1g)**.

M1 and M2 macrophages display distinct distributions across FAP disease progression

Macrophages play a crucial role in the homeostatic maintenance of the body through eradicating cytotoxic waste materials and vascular tissue regeneration[30-33]. However, the functions of two polarized states of macrophages M1 and M2 vary depending on the

microenvironment cues. For example, M1 macrophages can be tumor-resistant, while M2 macrophages can promote tumor growth[34,35] (**Fig. 2a**). We observe a higher proportion of M1 macrophages when compared with its polarized M2 counterpart within the normal and FAP mucosa. Conversely, M2 macrophages were found to increase in FAP polyps and adenocarcinoma/CRC samples. It has been documented that the ratio of M1: M2 macrophage is an important determinant towards the prognosis of colorectal cancer and other intestinal bowel disorders (IBDs)[36,37]. We observed an increase in M1: M2 macrophage ratio in normal mucosa and FAP mucosa and decrease in the above ratio was associated with FAP polyp and adenocarcinoma/sporadic CRC (**Fig. 2b).** We also observed that M1 macrophages mostly colocalize with activated CD4+ T cells rather than the CD4+ T cells (**Fig. 2c)**. While computing Pearson correlation coefficient for all the tissue samples involved, we find significant correlation between activated CD4+ T cells and M1 macrophages ($p = 0.034$) within normal and FAP mucosa when compared to that of FAP polyp and adenocarcinoma samples (**Fig. 2d)**. This observation aligns with previous studies, where M1 macrophages have been shown to regulate T cell activation by providing the required cytokines and other costimulatory signals[38-40].

Beta (β)-catenin is an important protein, which is involved in both gene transcription and coordination of cell-cell adhesion[41,42]. Previous studies have shown that overexpression of β-catenin is associated with various cancers such as colorectal adenocarcinoma, lung cancer, malignant breast tumors, and ovarian cancer[43-45]. Moreover, alterations in the localization and nuclear expression levels of β-catenin (i.e. nuclear accumulation) have been associated with malignant transformation by activating several downstream target genes such as TCF, and LEF1[46-48]. It has been shown that, unlike M1 macrophages, M2 macrophage polarization promotes β-catenin expression in murine macrophage-like RAW264.7 cells and alveolar macrophages[49]. Our results show that nuclear expression of β-catenin increases in the presence of a higher population of M2 macrophages in the FAP adenocarcinoma/sporadic CRC samples. We observe membranous expression of β-catenin in normal and FAP mucosa, where the M1 macrophage population is higher than the M2 counterpart (**Fig. 2e**).

Cancer cells, which require adequate supply of blood and nutrients, release angiogenic factors that encourage the growth of new blood vessels through a process called neo-angiogenesis. This process also involves a type III filamentous protein, vimentin, which helps in the migration, growth, and differentiation of endothelial cells lining the newly formed blood vessels[50,51]. Previously it has been shown that M2 macrophages induced by IL-4 and also neutrophils express the highest level of pro-MMP9 which stimulates angiogenesis *in vitro*[52]. We observe a significant increase in blood vessel density in the FAP affected tissues compared to normal mucosa (**Fig. 2f**) and also noticed the expression of vimentin protein along the endothelial lining of the newly formed blood vessels and microcapillaries (shown as branch formation), which are absent from mature blood vessels (**Fig. 2g**).

Regulatory T cells support proliferation of cancer stem cells within polyp microenvironment

The normal colonic stem cell niche at the base of the glandular crypt is responsible for homeostasis and repair of the intestinal epithelial layer[53-55]. CRC stem cells (CSCs) have similar characteristics to those of normal colonic stem cells; however, these cells differentiate aberrantly, contributing to the supply of bulk tumor cells depending on several microenvironmental cues[56-58]. In both FAP mucosa and FAP polyp samples, we observe stem-like cells within the glandular crypts. Moreover, we detect a significant increase in the percentage of stem-like cells expressing a CSC marker, SOX2, in the FAP polyps compared to the FAP mucosa samples (**Fig. 3a**)

Regulatory T (Treg) cells expressing the Foxp3 transcription factor play a critical role in promoting the stemness of gastric cancer cells through the IL13/STAT3 pathway[59,60] and also help in reducing overactive immune responses within the tumor microenvironment[61,62]. Within FAP polyps, we observe a significant increase in the percentage of memory T cells expressing Foxp3 indicating an overall increase in the Treg population (**Fig. 3b**). In order for effective cell-cell communication and for providing cytokines and interleukins (microenvironmental cues)[63,64] for the CSC survival and proliferation, Tregs have been shown to localize in the same region as the CSCs (**Fig. 3c)**.

Immunosuppressive microenvironment is found within FAP adenocarcinoma tumor 'nest'

Cancer cells are generated from the CSCs which ultimately expand out from the intestinal crypt region and invade other surrounding tissue regions. Using a tumor marker, carcinoembryonic antigen (CEA), we have detected a sequential increase in the expression of CEA marker across the FAP disease continuum. Normal mucosa did not express the tumor marker, while the highest percentage of cells expressing CEA protein was found within the tumor sample, as expected (**Fig. 3d)**. While imaging a FAP adenocarcinoma patient sample, we detect a whole tumor 'nest' embedded within the stromal compartment. The cancer cells within the 'nest' secrete angiogenic factors for tumor angiogenesis, needed for proliferation[65,66]. The immune cells, comprising mostly CD8+ T cells and CD4+ T cells, B cells, and NK cells have been found outside of the tumor 'nest' (**Fig. 3e)**. Density contour of the tumor cells and the surrounding immune cells reveal an immunosuppressive environment within the tumor 'nest' (**Fig. 3f**). We also detect tumor associated macrophages (TAMs) located at the tumor invasive front. It has been reported that TAMs also secrete various cytokines which contribute to the tumor angiogenesis process[67-69]. Interestingly, M1 macrophages have been seen at a distance from the tumor front, expressing inducible nitric oxide synthase (iNOS) (**Fig. 3g**) as part of macrophage inflammatory response[70-72] . Furthermore, CODEX imaging also allowed us to visualize various interesting interactions between the immune and the tumor cells happening near the tumor invasive front. During proliferation, cancer cells have been able to initiate an 'escape' by damaging the vascular endothelial cell lining of the tumor 'nest'. However, we observe a battery of immune cells confronting the escape, thereby preventing the cancer cells from migrating into the surrounding stroma. As a part of counter-effect, tumor cells have been seen expressing PD-L1 as an "adaptive immune mechanism" to escape anti-tumor responses[73,74] (**Fig. 3h)**.

Cancer associated fibroblasts (CAFs) play an essential role in FAP disease progression

The stromal compartment comprises basement membrane, fibroblasts, extracellular matrix, immune cells, and vasculature basically maintains both normal epithelial tissues and their malignant counterparts[75] (**Fig. 4a**). Previous findings have shown that changes within the stromal microenvironment at the tumor invasion front lead to the transdifferentiation of fibroblasts to CAFs. Several cancer-derived cytokines such as transforming growth factor-β (TGF- β) are responsible for such transformation[76,77].

A significant portion of the reactive tumor stroma comprises CAFs, which play a crucial role in tumor progression[78,79]. Various stromal markers including COL6A2, CD90, MYH11, α-SMA, VIM, PDPN, VCAN were used to spatially locate the various categories of the fibroblast population within normal mucosa and FAP tissue samples (**Fig 4b & c**). We detected several groups of fibroblasts such as fibroblasts responsible for Epithelial-to-Mesenchymal transition, activated fibroblasts, inflammatory fibroblasts, and CAFs within the precancer and tumor

stroma, which shows higher expression across the FAP disease progression. In particular, the expression of inflammatory fibroblast and CAFs is higher in adenocarcinoma/sporadic CRCs. As expected, we observe a lower expression of normal fibroblast in the FAP diseased tissue samples, while higher expression is observed in normal mucosa (**Fig. 4d**). We further inquired if CAF is potentially responsible for inflammation in the FAP affected colorectal tissue samples. In order to understand, both FAP polyps and tumor samples were stained with VCAN (inflammatory marker), PDPN (CAF marker) and COL6A2 (normal fibroblast/basal lamina marker) and imaged. A surface plot of the marker intensity has been generated for each of these markers followed by computing the Vansteelsen's cross correlation coefficient (CCF), which was measured on those surface plots. Vansteelsen's CCF shows how the Pearson coefficient changes after shifting the red image voxel over green image voxel. By observing the shape of the CCF plot as a function of this shift, it can be determined if the signals of the two channels are actually positively correlated[80]. We find that the overlap CCF between PDPN (CAF marker) and VCAN (inflammatory marker) increases while the overlap CCF between PDPN and COL6A2 decreases in FAP adenocarcinoma/CRC samples indicating that CAFs are present in close proximity to the inflammatory region of the FAP affected tissue for promoting tissue malignancy and are not correlated with normal fibroblasts (**Fig. 4e**).

CODEX imaging also revealed how stromal CAFs invade the epithelial layer in FAP tumor samples leading to further spreading of tumors. Basically, normal mucosa has a continuous lining of the basal membrane which gets disrupted when CAFs migrate towards them. In order to support this process, the myofibroblasts present near the basal membrane start expressing α-SMA which is required for matrix contraction and remodeling[81] **(Fig. 4f).** Moreover, it has been observed that CAFs also affect the expression of E-cadherin, which is a membrane protein that helps maintain the epithelial barrier by joining neighboring cells together to form tissues[82]. In our CODEX imaging data, we detect CAFs inhibiting the expression of E-cadherin on the glandular epithelial cells which are along the CAF migratory path **(Fig. 4g)**. In contrast, the glandular cells which are further away from the CAFs migratory route remain unaffected by the effect of CAFs and express E-cadherin.

TILs are an integral part of the body's immune system, identifying and eliminating abnormal cells, including cancer cells[83,84]. In FAP adenocarcinoma, we observe a high CAF population, which inhibits the migration of TILs into the tumor stroma. In contrary, a low CAF population within a sporadic CRC sample is less resilient to TILs **(Fig. 4h)**. Overall, the percentage of TILs comprising CD4+ T cell, CD8+ T cell, and plasma B cells decreased with increase in CAF population. Interestingly, CAF had no effect on the Treg population within the tumor stroma **(Fig. 4i)**. However, this is expected as Tregs often play an immunosuppressive role helping immune escape of tumors in the body[85-87].

Neighborhood analyses between adjacent FAP mucosa and FAP polyp show differences in spatial location of cells based on cell-cell functionality

In order to understand intercellular interactions and cellular densities, we performed neighborhood analyses[88] from FAP mucosa and FAP polyp samples using methods described in Hickey et al (2022). Heatmaps reflecting the enrichment of cell types that preferentially co-localize with one another within different regions are shown in Figure 5. In FAP mucosa, the endothelial cells and CD4+ T cells reside within the same region. Endothelial cell (EC)-T cell interactions play a significant role in the regulation of the immune system, where the ECs control T cell recruitment and activation[89,90]. Similarly, monocytes and neutrophils colocalize with lymphatic ECs while CD8+ T cells were found near the enterocytes (**Fig. 5a, left panel**). In FAP polyp samples, macrophages and CD4+ T cells colocalize within a region. Neutrophils also migrate towards the intraepithelial zone and join CD8+ T cells (IELs). Moreover, mast cells

colocalize with lymphatic endothelial cells and are enriched in different regions of the polyp tissue (**Fig. 5a, right panel)**. We also observe a higher number of interactions between various cell types in FAP polyps compared to that of FAP mucosa (**Fig. 5b**). We detect lymphoid follicles found within adjacent FAP mucosa consisting of B cells inside the lymphoid follicle and memory T cells outside the lymphoid follicle (**Fig. 5c**). Ten regions were detected in both FAP mucosa and FAP polyp samples using neighborhood analyses. In FAP mucosa, where the severity of the cancer cells expressing PD-L1+/CEA+ tumor markers is low, we observe immune cells within the same region as that of the tumor cells. These cells are probably present to counteract the cancer cells. Unlike FAP mucosa microenvironment, an immunosuppressive microenvironment is created where the PD-L1+/CEA+ expressing cells and immune cells segregate into separate regions (**Fig. 5d**). Several interesting differences in terms of cell-cell localization (heatmap) were found in FAP polyps when compared to that of FAP mucosa samples. It has been seen that, as the FAP disease progresses (i.e. within FAP polyp samples), the M2 macrophage started to show several interactions with other cell types, specifically CD4+ T cells, B cells and M1 macrophages. Similar interactions were not present in FAP mucosa. Moreover, CD8+ T cells have been shown to interact and localize in the same region as that of CEA/PD-L1 and not CD4+ T cells (which was previously shown to interact in FAP mucosa). Unlike FAP mucosa, it has been also seen that memory T cells interact with CEA+ cancer cells as tissue-resident memory T cells are responsible for tumor immunity (**Fig. 5e**).

Discussion

Premalignant events lead to abnormal changes responsible for triggering cancer precursors that favor the initiation of a tumor[91,92]. Therefore, studying the precancer environment is crucial for earlier diagnosis, novel interventions, and risk stratification thereby improving tumor risk management and leading to potential prevention strategies. Previous research on colorectal cancer biology mainly focused on advanced-stage tumors[93-95] and has largely disregarded pre-cancer events. Even though snRNA and ATAC sequencing helps understand differences between individual cells, cellular heterogeneity and complex biological systems, both these techniques dissociate the cells, thereby losing important spatial information. Our CODEX multiplexed imaging fills the gap by spatially mapping single cells across the FAP disease continuum, thereby providing information about how cells organize and interact across the pre-cancer microenvironment and inform key changes during the disease progression.

Analysis of cell type composition reveals an increase in stem-like cells, CAFs, Tregs, M2 macrophages and decrease in NK cells, M1 macrophages, goblet cells across the disease continuum. A pre-cancer microenvironment that encourages the growth of cancer cells is probably favored by the observed changes in cell type composition across the disease continuum. For example, the decrease in goblet cells in intestinal crypts and increase in CAFs, Tregs and exhausted T cells in the stroma overall favor an immunosuppressive environment within premalignant polyps and adenocarcinoma. Identifying the similar cell types within normal and FAP mucosa shows different cell type composition, which are unfavorable for tumor growth. The CD4+/CD8+ ratio is an important indicator of the overall strength of the immune system within a patient's body. Higher CD4+ T cells over CD8+ T cells contribute to a relatively stronger immune system, while the reverse indicates a weaker system[24,25]. Within the immune cell population, we observe a decrease in CD4+/CD8+ T cell ratio during the FAP disease progression. The CD8+ T cells positioned at the interface of the intestinal lumen of the colon and external environment not only help in balancing immune tolerance but also protect the fragile intestinal barrier from invasion[26]. It could be also possible that patients with low CD4+/CD8+ ratio have a better clinical course, with significantly higher 5-year survival[96]. Within the epithelial compartment, we observe a higher percentage of mucin producing cells in females compared to the male patients. Mucin glycoproteins protect epithelial lining of the GI tract[27]. We

suspect that the presence of this protective layer could be one of the plausible explanations as to why male patients in our study developed FAP adenocarcinoma.

We also find that the increase in stem-like cell population within precancer polyps has no correlation to donor's age. This is expected because self-renewal capabilities of stem-like cells divide to create more stem cells in advanced polyps, which is essential for maintaining stemness and tumor formation. However, signals from other cell types in the vicinity also determine whether stem cells will self-renew, differentiate or remain quiescent. In our study, we find Tregs localize near stem-like cells within FAP polyps and CRCs, which play a critical role in promoting the stemness, possibly by providing cytokines and interleukins for the CSC survival and proliferation. Vascular endothelial cells and TAMs have been also present near the CSCs, which further creates a favorable environment for stem cell proliferation. Recent studies involving single-cell RNA sequencing of gastric cancer and adjacent tissues found that Tregs were recruited to gastric cancer tissues and have further demonstrated that Tregs promote the stemness of gastric cancer cells through the IL13/STAT3 pathway[59,60]. As a result, we find an increase in the fraction of stem-like cells expressing cancer marker, SOX2, within polyps compared to FAP mucosa. Therefore, it would be interesting to see if blocking the interaction between Tregs and CSCs within the precancer microenvironment could be a potential approach in the treatment of CRC. Within the immune microenvironment, both resident and recruited macrophages are key modulators during tumor progression which have several immunoregulatory functions. Similar to CD4+:CD8+ T cell ratio, M1:M2 macrophage ratio also decreases along with the FAP disease continuum. We find more M2 polarization occurring in advanced polyps than normal and FAP mucosa. This is expected as M1 is anti-tumorigenic and M2 is pro-tumorigenic[34]. Moreover, we observe higher M2 polarized macrophage population tends to favor nuclear expression of β-catenin, which is normally found in the epithelial cell membrane, where it helps with cell-to-cell adhesion. In the nucleus, β-catenin is associated with transcription factors from the TCF/Lef family and drives transcription of Wnt/β-catenin target genes leading to malignancy[41]. Previously it has been shown that mRNA/protein levels of β-catenin, Axin2, and c-Myc were significantly increased in M2 macrophages compared with that in M0 or M1 macrophages[97]. Hence, interfering with the macrophage polarization during the precancer stage could be a turnaround step preventing nuclear localization of β-catenin, thereby curbing transcription of malignant genes.

Solid tumors require sufficient blood supply to grow beyond a few millimeters in size. It has been shown that nearby normal cells are also stimulated by tumors to produce angiogenesis signaling molecules[65,66]. We find an increase in vasculature and microcapillaries within FAP polyps and tumors compared to normal and FAP mucosa. Most studies have reported angiogenesis once the invasive adenocarcinoma has been established[98-101]. However, we find that even in premalignant stages, such as FAP mucosa and polyps, epithelial cells have increased proliferation and therefore would be expected to require increased blood supply. Therefore, targeting blood vessels in the premalignant stage with angiogenesis inhibitors such as, Axitinib (Inlyta®), Bevacizumab (Avastin®),Cabozantinib (Cometriq®) that specifically recognize and bind to vascular endothelial growth factor (VEGF) could be an effective route.

Among the other fibroblasts that we have detected within the stromal compartment of pre-cancer polyps and tumors, CAFs have been a central component of the tumor microenvironment, as they not only interfere with cell-cell adhesion but also interact with cancer cells via secreted molecules, influence cancer cells via extracellular matrix (ECM) remodeling and immune cell infiltration[102]. We have shown that CAFs are present near the inflammatory regions and inhibit the expression of E-cadherin protein, thereby interrupting the cell-cell adhesion feature. Moreover, CAFs have been shown to influence immune infiltration. Our imaging data shows that higher CAF populations in the stromal regions are only able to limit the entry of CD4+ T cells, CD8+ T cells, and plasma B cells into the tumor microenvironment, which

results in the creation of an immunosuppressive environment. Moreover, when tumor: stroma ratio (TSR) was calculated, 2 FAP adenocarcinomas have shown higher stromal content compared to 4 sporadic CRCs, which have shown low to medium stromal content (**Supplementary Fig. 5**). Usually, high stroma is associated with poor disease prognosis. Therefore, both CAF and high stromal content might have restricted the immune cell infiltration. Despite the fact that CAFs have long been thought to be a key factor in the development of cancer and thus make an appealing therapeutic target, most clinical trials that attempt to target CAFs have failed[103,104]. Though the current research focuses on finding new CAF subsets that promote tumors and ways to specifically target them, it's important to note that finding tumor-suppressive CAF populations and how to maintain their homeostatic balance will also be valuable as future stroma-targeted therapies. Consequently, there is a growing understanding that therapeutic approaches with the potential to improve patient survival include normalizing or re-engineering the tumor stroma into a quiescent state or even tumor-suppressive phenotypes. Based on functionality, neighborhood analyses between neighboring FAP polyps and mucosa reveal differences in the spatial location of cells. Heatmaps that display fold change of distinct cell types within various regions, where specific cell types colocalize due to potential functional significance have been generated. When macrophages and CD4+ T cells colocalize in an area of FAP polyp samples, they essentially activate one another and get ready to fight any invasive pathogens. To strengthen the immune response even more, neutrophils also move into the intraepithelial zone where they associate with CD8+ T cells (IELs). Additionally, mast cells migrate to various areas of the polyp tissue and colocalize with lymphatic endothelial cells. We find immune cells in the same area as the tumor cells in the FAP mucosa, where the cancer cells that express PD-L1+/CEA+ tumor markers are not as severe. Most likely, these cells are here to fight off the cancer cells. However, in advanced polyps, cancer cells create an immunosuppressive microenvironment by keeping the immune cells at a distance.

Overall, our single-cell spatial imaging data demonstrates the changes in cell type composition throughout initiation of polyp formation from mucosa and the malignant transition of polyps into CRC, offering insights into the organization and interactions of cells inside the pre-cancerous milieu and driving important modifications during the course of the disease. We also discussed a few potential interventions that could be deployed within the pre-cancer microenvironment, in order to curb tumor initiation and metastasis. This research is expected to have a significant impact on understanding the FAP pre-cancer microenvironment, as well as early stages of sporadic CRCs and other gastrointestinal malignancies, which will facilitate the implementation of early treatment and potential preventive interventions.

Methods

Tissue collection and processing

The Stanford University Institutional Review Board and the Washington University Institutional Review Board (normal mucosa from deceased organ donors) have both approved this study, which conforms with all applicable ethical regulations. For every donor participant, the next-of-kin provided written informed consent. All of the FAP patient tissues used in this study were procured from colons explanted via total colectomy procedures. The patient colons were taken directly from the surgical suite to the Stanford Hospital pathology gross room where they were quickly rinsed and bisected with surgical scissors longitudinally on a room temperature cutting board typically used in a pathology gross room. Polyp-adjacent normal mucosa (absent any

visible polyps) and polyp tissues were carefully dissected from the colon, measured, stored in cryovial tubes, and flash frozen by placing the samples in cryotubes directly into liquid nitrogen. Polyps that had a maximum diameter in any direction that was larger than 10 mm were considered "large", between 10 mm and 5 mm were "medium", and less than 5 mm were considered "small". However, these size categories did not apply to normal mucosa. All polyps greater than 10mm in diameter were frozen sectioned, H&E stained and underwent histopathologic review by project pathologists to assess percentage of normal vs dysplastic tissue and presence of dysplasia by grade (low grade dysplasia vs high grade dysplasia). Polyps less than 10mm in size were not uniformly subjected to this histopathologic analysis, due to the low likelihood of high-grade dysplasia in this size of polyps (PMID: 20304097) and the very limited amount of tissue available for analysis. To record the exact location on the colon where the different tissue samples came from for patients A001, A002, A014, A015, we replaced each tissue sample with a numbered thumb-tack and took pictures of the bisected and pinned open colonic lumen. Using a ceramic mortar and pestle, we pulverized the flash frozen samples in liquid nitrogen to create a fine powder or small chunks as input to each multi-omic assay. For a subset of tissue samples, flash frozen polyps and colorectal mucosa were embedded in frozen OCT media and serial sectioned for 2D structural analyses. Once flash frozen or embedded in frozen OCT media, tissue was preserved at -80 degrees C until utilized for analyses.

CODEX antibody conjugation and antibody panel creation

CODEX multiplexed imaging was carried out using the staining and imaging protocol outlined in the manufacturer's user manual. Antibody panels were designed to include targets that distinguish intestinal epithelial and stromal cell subtypes, as well as innate and adaptive immune system cells and cancer cells. Detailed panel information is provided in **Supplementary Table 3.** Each antibody was conjugated to a unique oligonucleotide barcode, and the tissues were stained with the antibody-oligonucleotide conjugates. We verified that the staining patterns in positive control tonsil or intestine tissues, which matched those previously established for immunohistochemistry. Prior to being evaluated collectively in a single CODEX multicycle, antibody-oligonucleotide conjugates were first evaluated with immunofluorescence assays, where the signal-to-noise ratio was also assessed.

Preparing tissue samples for CODEX imaging

Imaging data were gathered from twenty human donors, each of whom represented a dataset. Each dataset contains tissue samples from pre-cancer polyps and adenocarcinoma/CRC collected from different sections of the colon (sigmoid, descending, transverse and ascending). The tissues were individually frozen in Optical Cutting Temperature (OCT) molds and then sectioned at a width of 8μm using a cryostat, assembled on Leica Superfrost adhesive slides and were stored at -80 °C, until needed. The tissue slides were processed according to the manufacturer's protocol. Briefly, the slides were obtained from the freezer on the day of the CODEX experiment and placed on 1-2 cm Drierite beads for 2 mins, followed by 10 mins incubation in acetone. The acetone was dried by placing the slides facing up in a humid chamber for 2 mins. The tissue sections were incubated in 5 ml Hydration buffer for 2 mins (twice) and fixed using 1.6% Paraformaldehyde (PFA) for 10 mins, after which the fixative was thoroughly removed by rinsing in the same Hydration buffer. The slides were incubated in a 5 ml staining buffer for 20 mins. In the meantime, a stock solution of CODEX blocking buffer was prepared by mixing 362 μl of Staining buffer and 9.5 μl each of the company's proprietary buffers namely N, G, J, S blockers (per 2 samples). The volume of antibody per sample slide

was calculated and subtracted from the CODEX blocking buffer. An antibody cocktail solution was prepared by pipetting each antibody into the CODEX blocking buffer. The sample slides were placed in the humidity chamber and the antibody cocktail staining solution (200 µl per tissue sample) was dispensed on the slide and incubated for 3 hours at room temperature. Subsequently, unbound antibodies were removed by rinsing the slides in 5 ml Staining buffer for 2 mins (twice). The samples were placed in post-staining fixative solution (1 ml of 16% PFA + 9 ml of Storage buffer) for 10 mins and washed thoroughly with 1x Phosphate buffer saline (PBS) to remove the fixative. Subsequently, the tissue sections were fixed with ice cold methanol for 5 mins at 4 °C and washed with 1x PBS. The samples were incubated in a final fixative reagent (20 µl of CODEX fixative reagent + 1 ml of 1x PBS) for 20 mins, washed thoroughly with 1x PBS before placing in the storage buffer (up to 2 weeks at 4 °C). In the meantime, a reporter plate for interrogating the corresponding barcoded-antibodies was prepared by adding nuclease-free water, 10x CODEX buffer, assay reagent, and nuclear stain. Two forty microliters of the stock solution were dispensed into individual wells followed by 5 µl of the corresponding reporter dyes. The reporter solutions were mixed and pipetted into individual wells of a 96-well plate, covered with a foil seal, and stored at 4 °C for imaging.

CODEX multiplexed imaging

A CODEX microfluidic instrument also known as Phenocycler Fusion (Akoya Biosciences Inc., CA, USA) integrated with an inverted fluorescence microscope through a custom stage insert was used to automate CODEX buffer exchange and image acquisition. The tissue slides were placed on the stage insert and imaged with multiple cycles of CODEX imaging. The first and the last cycles were basically blank cycles and also used for image registration and image alignment. Tissue sections were imaged in a 5x7 tiled acquisition at 377 nm/pixel resolution and 9 z-planes per tile. The tile overlap was preset at 30%.

CODEX data processing and visualization

The image data and experiment.json files were transferred to CODEX Analysis Manager (CAM) for further processing of the raw images, which were then subjected to background subtraction, shading correction, along with deconvolution to remove out-of-focus light using a Microvolution software available from http://www.microvolution.com/. After drift-compensation and stitching, the best focal plane of vertical image stacks collected at each acquisition were chosen for cell segmentation using a gradient-tracing watershed algorithm (Akoya built-in software) on the nuclear staining (radius set to 6 pixels). The processed images were visualized and analyzed using CODEX Multiplex Analysis Viewer (MAV) installed as an extension within ImageJ software (https://imagej.nih.gov/ij/). MAV enables visualization, annotation, and analysis of cell populations from CODEX imaging data. For each cell in the imaged tissue, MAV generates spatial coordinates and measures the integrated signal intensity for each antibody. Occasionally, while using manual gating, some cell segmentation noise that could affect cell type identification have been revealed but using Leiden-based unsupervised clustering, followed by over-clustering and manually overlaying the resultant cell type clusters to the image resulted in much accurate identification of cell types. Both CODEX MAV and Qupath software can be downloaded from https://help.codex.bio/codex/mav/installation/download-and-install and https://qupath.github.io/ . Alternatively, Qupath platform was also used for image data visualization and performing cell measurements followed by histo-cytometric multidimensional analysis pipeline (CytoMAP) to analyze the processed images (https://gitlab.com/gernerlab/cytomap). Once the paired.csv files were saved in Qupath, the

annotated cell for every dataset was imported into CytoMAP. All of these include the spatial locations, gate definitions, and cell statistics for every cell object. This spatial analysis technique extracts and quantifies information about preferential cell-cell associations, global tissue structure, and cellular spatial positioning using a range of statistical techniques.

Cell type analysis

The identification of cell types was carried out using previously described methods[20,105]. Briefly, DAPI+ cells were gated to select nucleated cells, and then protein markers used for clustering were normalized using z-normalization. Then the data were overclustered with X-shift clustering function within CODEX MAV program or Leiden-based clustering embedded within the Seurat package (version 5.1.0.). Seurat performs uniform manifold approximation and projection (UMAP), computes cell clusters and scales the data to observe variations in antigen expression on cells. The above steps were performed based on an in-depth analysis of marker intensity associated with cell types and its localization within the tissue and referred to the published images for that specific antibody. Based on the location within the image and the average cluster protein expression, a cell type was assigned to each cluster.

Cell neighborhood analysis

Using raster scanned neighborhood analysis, CytoMAP determines the local cell composition inside a spherical (3D data) or circular (2D data) area/volume in the tissue. This function will treat the data as effectively 2D and use a cylindrical neighborhood window if the z dimensionality of the data is non-zero but the z thickness is less than the neighborhood radius. This function determines the total number of cells in each neighborhood as well as the maximum fluorescence intensity (MFI) of each channel. With a half of the user-defined radius separating the neighborhood centers, the neighborhoods are uniformly spaced out in a grid pattern throughout the tissue. Then, additional analysis (e.g., local cellular densities, cell-cell associations) can be performed using the neighborhood data.

Classify neighborhoods Into regions

The cell neighborhoods have been further grouped into regions. Multiple types of neighborhood information are used to define tissue regions using CytoMAP's *region* function. This comprises the composition (number of cells divided by the total number of cells in each neighborhood), the raw number of cells per neighborhood, and the standardized number of cells of each phenotype in each neighborhood (number of cells minus mean number of cells, divided by the standard deviation of the number of cells in each neighborhood across the dataset). The number of regions and the neighborhood clustering were automatically determined by default using the Davies-Bouldin function. Once the network parameters were determined, the network was trained on the neighborhood data using MATLAB's *train* function. This assigns a cluster number to each neighborhood. At the beginning of the selforgmap algorithm, NR "neurons" are scattered throughout the data. Then, in order to match the data's landscape, it iteratively shifts the neurons' positions closer to the data. In this case, the position is topological within the cell composition data rather than spatial. Next, each neighborhood's closest neuron is located, leading to the clustering of the neighborhoods. Using CytoMAP's Edit Region Colors function, the individual regions' arbitrary color designations were altered for visual aids. With CytoMAP's Heatmap Visualization feature, the color-coded neighborhoods' composition was plotted. By creating a new figure in CytoMAP, plotting the neighborhood positions, and choosing the

regions for the 'c' axis to color-code the neighborhoods according to region type, the spatial distribution of the regions was made visible.

Cell-Cell Correlation Analysis

Certain cell populations preferentially associate with one another, or conversely avoid one another, based on the local cell density within individual neighborhoods, which can be used to correlate the location of different cell types. The number of cell or object types within the scanned neighborhoods was calculated using the Pearson correlation coefficient by the correlation, or corr function, within CytoMAP. This information is then graphed on a heatmap plot. This correlation analysis can be carried out on a number of samples, covering entire tissues or just specific areas of the tissues. This is significant because different tissue compartments may have different associations between cells.

Data availability

Raw and processed CODEX image data generated in this study have been deposited to Synapse (www.synapse.org/) and are indexed on the Human Tumor Atlas Network (HTAN) Data Portal. The list of study files can be retrieved by accessing the HTAN Data Portal (https://data.humantumoratlas.org/explore) and filtering for Atlas: “HTAN Stanford” AND Assay: “CODEX”.

Code availability

Codes for processing the single-cell CODEX imaging data using Akoya’s pipeline such as CODEX MAV and Qupath can be downloaded from https://help.codex.bio/codex/mav/installation/download-and-install and https://qupath.github.io/ respectively. CytoMAP scripts for analyzing the processed images and neighborhood analysis can be found at https://gitlab.com/gernerlab/cytomap. Seurat pipeline for analyzing the single cell imaging data can be found at https://cran.r-project.org/web/packages/Seurat/index.html.

References

1. Cooper GM. The Cell: A Molecular Approach. 2nd edition. Sunderland (MA): Sinauer Associates; 2000. The Development and Causes of Cancer.

2. Zhang S., et al. Tumor initiation and early tumorigenesis: molecular mechanisms and interventional targets. ***Sig Transduct Target Ther*** 9, 149 (2024).

3. Sandouk F, et al., Precancerous lesions in colorectal cancer. ***Gastroenterol Res Pract***. 457901 (2013).

4. Gibson JA, Odze RD. Pathology of premalignant colorectal neoplasia. ***Dig Endosc***. 3:312-323 (2016).

5. Vogelstein B., et al. Genetic alterations during colorectal-tumor development. ***N Engl J Med***. 319(9):525-532 (1988).

6. Duan B., et al. Colorectal Cancer: An Overview. ***Gastrointestinal Cancers***. Brisbane (AU): Exon Publications (2022).

7. Rawla P., et al. Epidemiology of colorectal cancer: incidence, mortality, survival, and risk factors. ***Prz Gastroenterol***. 14(2):89-103 (2019).

8. Parker T.W., Neufeld, K.L. APC controls Wnt-induced β-catenin destruction complex recruitment in human colonocytes. ***Sci Rep*** 10: 2957 (2020).

9. Stamos JL, Weis WI. The β-catenin destruction complex. ***Cold Spring Harb Perspect Biol.*** 5(1):a007898 (2013).

10. Cai J., et al. β-Catenin destruction complex-independent regulation of Hippo-YAP signaling by APC in intestinal tumorigenesis. ***Genes Dev.*** 29(14):1493-1506 (2015).

11. Al-Sukhni W., et al. Hereditary colorectal cancer syndromes: familial adenomatous polyposis and lynch syndrome. ***Surg Clin North Am***. 88(4):819-844 (2008).

12. Jasperson KW, Tuohy TM, Neklason DW, Burt RW. Hereditary and familial colon cancer. ***Gastroenter.***138(6):2044-2058 (2010).

13. Bujanda L., et al. Malignant colorectal polyps. ***World J Gastroenterol.*** 16(25):3103-3111 (2010).

14. Manjula J., et al. Screening for Cancerous and Precancerous Conditions of the Colon, ***Primary Care: Clinics in Office Prac.*** 383(3): 449-468 (2011).

15. Islam R.S., et al. Gastric polyps: a review of clinical, endoscopic, and histopathologic features and management decisions. ***Gastroenterol Hepatol***. 9(10):640-651 (2013).

16. Chen B., et al. Differential pre-malignant programs and microenvironment chart distinct paths to malignancy in human colorectal polyps. ***Cell***. 184(26):6262-6280 (2021).

17. Becker W.R., et al. Single-cell analyses define a continuum of cell state and composition changes in the malignant transformation of polyps to colorectal cancer. ***Nat Genet.*** 54, 985–995 (2022).

18. Rozenblatt-Rosen et al. The Human Tumor Atlas Network: Charting Tumor Transitions across Space and Time at Single-Cell Resolution ***Cell.*** 181(2):236 – 249 (2020).

19. Hickey J.W., et al. Strategies for Accurate Cell Type Identification in CODEX Multiplexed Imaging Data. ***Front Immunol.*** 12:727626 (2021).

20. Goltsev Y., et al. Deep Profiling of Mouse Splenic Architecture with CODEX Multiplexed Imaging. ***Cell***.174(4):968-981 (2018).

21. Ahmed A.S., et al. Effect of aging on stem cells. ***World J Exp Med.*** 7(1):1-10 (2017).

22. Han S., et al. Tumour-infiltrating CD4(+) and CD8(+) lymphocytes as predictors of clinical outcome in glioma. ***Br J Cancer.*** 110(10):2560-2568 (2014).

23. Idos G.E., et al. The Prognostic Implications of Tumor Infiltrating Lymphocytes in Colorectal Cancer: A Systematic Review and Meta-Analysis. ***Sci Rep.*** 10(1):3360. (2020)

24. Garrido-Rodríguez V., et al. Immunological features beyond CD4/CD8 ratio values in older individuals. ***Aging.*** 13(10):13443-13459 (2021).

25. Idos G.E., et al. The Prognostic Implications of Tumor Infiltrating Lymphocytes in Colorectal Cancer: A Systematic Review and Meta-Analysis. ***Sci Rep.*** 10(1):3360 (2020).

26. Konjar Š., et al. Intestinal Barrier Interactions with Specialized CD8 T Cells. ***Front Immunol.*** 8:1281 (2017)

27. Cornick S., et al. Roles and regulation of the mucus barrier in the gut. ***Tissue Barriers.*** 3(1-2):e982426 (2015).

28. Pelaseyed T., et al. The mucus and mucins of the goblet cells and enterocytes provide the first defense line of the gastrointestinal tract and interact with the immune system. ***Immunol Rev.*** 260(1):8-20 (2014).

29. Kim Y.S., Ho S.B. Intestinal goblet cells and mucins in health and disease: recent insights and progress. ***Curr Gastroenterol Rep.*** 12(5):319-330 (2010).

30. Matthew D.P., et al. Macrophages in health and disease. ***Cell***, 185(23):4259-4279 (2022).

31. Hirayama D., et al. The Phagocytic Function of Macrophage-Enforcing Innate Immunity and Tissue Homeostasis. ***Int J Mol Sci***.19(1):92 (2017).

32. Chen S., et al. Macrophages in immunoregulation and therapeutics. ***Signal Transduct Target Ther.*** 8(1):207 (2023).

33. Wculek, S.K., et al. Metabolism of tissue macrophages in homeostasis and pathology. ***Cell Mol Immunol.*** 19, 384-408 (2022).

34. Huang R., et al. The role of tumor-associated macrophages in tumor immune evasion. ***J Cancer Res Clin Oncol.*** 150(5):238 (2024).

35. Zhang Q., Sioud M. Tumor-Associated Macrophage Subsets: Shaping Polarization and Targeting. ***Int J Mol Sci.*** 24(8):7493 (2023).

36. Zhang K., et al. Macrophage polarization in inflammatory bowel disease. ***Cell Commun Signal.*** 21(1):367 (2023).

37. Yip J.L.K., et al. The Role of Intestinal Macrophages in Gastrointestinal Homeostasis: Heterogeneity and Implications in Disease. ***Cell Mol Gastroenterol Hepatol.***12(5):1701-1718 (2021).

38. Guerriero J.L. Macrophages: Their Untold Story in T Cell Activation and Function. ***Intl Rev of Cell and Mol Biol.*** 34273-34293 (2019).

39. Doherty T.M. T-cell regulation of macrophage function. ***Current Opinion in Immunol.*** 7(3):400-404 (1995).

40. Pozzi L-A. M, et al. Both Dendritic Cells and Macrophages Can Stimulate Naive CD8+ T Cells In Vivo to Proliferate, Develop Effector Function, and Differentiate into Memory Cells. ***J Immunol.*** 175(4):2071-2081 (2005).

41. Valenta T., et al. The many faces and functions of β-catenin. ***EMBO J.*** 31(12):2714-2736 (2012).

42. Brembeck F.H. et al. Balancing cell adhesion and Wnt signaling, the key role of beta-catenin. ***Curr Opin Genet Dev.*** 6(1):51-59 (2006).

43. Shang S., et al. The regulation of β-catenin activity and function in cancer: therapeutic opportunities. ***Oncotarget.*** 8(20):33972-33989 (2017).

44. Zhao H., et al. Wnt signaling in colorectal cancer: pathogenic role and therapeutic target. ***Mol Cancer.*** 21:144 (2022).

45. Zhan T., et al. Wnt signaling in cancer. ***Oncogene*** 36, 1461-473 (2017).

46. Ramakrishnan A.B., Cadigan K.M. Wnt target genes and where to find them. ***F1000Res.*** 6:746 (2017).

47. Pai S.G., et al. Wnt/beta-catenin pathway: modulating anticancer immune response. ***J Hematol Oncol*** 10:101 (2017).

48. Cadigan K.M., Waterman M.L. TCF/LEFs and Wnt signaling in the nucleus. ***Cold Spring Harb Perspect Biol.*** 4(11):a007906 (2012).

49. Feng Y., et al. Wnt/β-Catenin-Promoted Macrophage Alternative Activation Contributes to Kidney Fibrosis. ***J Am Soc Nephrol.*** 29(1):182-193 (2018).

50. Ridge K.M., et al. Roles of vimentin in health and disease. ***Genes Dev.*** 36(7-8):391-407 (2022).

51. Shakhov A.S., Alieva I.B. The "Third Violin" in the Cytoskeleton Orchestra-The Role of Intermediate Filaments in the Endothelial Cell's Life. ***Biomedicines.***10(4):828 (2022).

52. Krzyszczyk P., et al. The Role of Macrophages in Acute and Chronic Wound Healing and Interventions to Promote Pro-wound Healing Phenotypes. ***Front Physiol.*** 9:419 (2018).

53. Hu D., et al. Recent advances in understanding intestinal stem cell regulation. ***F1000Res.*** 8 (2019).

54. Santos A.J.M., et al. The Intestinal Stem Cell Niche: Homeostasis and Adaptations. ***Trends Cell Biol.*** 28(12):1062-1078 (2018).

55. Pastuła A., Marcinkiewicz J. Cellular Interactions in the Intestinal Stem Cell Niche. ***Arch Immunol Ther Exp***. 67(1):19-26 (2019).

56. Abdul K.F.J., et al. Colon cancer stem cells. ***Gastrointest Cancer Res.*** 16 (2010).

57. Ayob A.Z., Ramasamy T.S. Cancer stem cells as key drivers of tumour progression. ***J Biomed Sci*** 25:20 (2018).

58. Hervieu C., et al. The Role of Cancer Stem Cells in Colorectal Cancer: From the Basics to Novel Clinical Trials. ***Cancers.*** 13(5):1092 (2021).

59. Zhao R., et al. TNF+ regulatory T cells regulate the stemness of gastric cancer cells through the IL13/STAT3 pathway. ***Front Oncol.*** 13:1162938 (2023).

60. Wang Y., et al. Complex Role of Regulatory T Cells (Tregs) in the Tumor Microenvironment: Their Molecular Mechanisms and Bidirectional Effects on Cancer Progression. ***Int. J. Mol. Sci.*** 25:7346 (2024).

61. Qiu Y., et al. FOXP3+ regulatory T cells and the immune escape in solid tumours. ***Front Immunol.*** 13:982986 (2022).

62. Tie Y., et al. Immunosuppressive cells in cancer: mechanisms and potential therapeutic targets. ***J Hematol Oncol.*** 15: 61 (2022).

63. Cho I., et al. Treg regulation of the epithelial stem cell lineage. ***J Immunol Regen Med.*** 8:100028 (2020).

64. Plaks V., et al. The cancer stem cell niche: how essential is the niche in regulating stemness of tumor cells? ***Cell Stem Cell.*** 16(3):225-238 (2015).

65. Nishida N., et al. Angiogenesis in cancer. ***Vasc Health Risk Manag.*** 2(3):213-219 (2006).

66. Saman H., et al. Inducing Angiogenesis, a Key Step in Cancer Vascularization, and Treatment Approaches. ***Cancers.*** 12(5):1172 (2020).

67. Larionova I., et al. New Angiogenic Regulators Produced by TAMs: Perspective for Targeting Tumor Angiogenesis. ***Cancers.*** 13(13):3253 (2021).

68. Chen Y., et al. Tumor-associated macrophages: an accomplice in solid tumor progression. **J Biomed Sci.** 26:78 (2019).

69. Ribatti D. et al. Macrophages and tumor angiogenesis. ***Leukemia.*** 21:2085-2089 (2007).

70. Palmieri E.M., et al. Nitric Oxide in Macrophage Immunometabolism: Hiding in Plain Sight. ***Metabolites.*** 10(11):429 (2020).

71. Palmieri E.M., et al. Nitric oxide orchestrates metabolic rewiring in M1 macrophages by targeting aconitase 2 and pyruvate dehydrogenase. ***Nat Commun.*** 11:698 (2020).

72. Xue Q., et al. Regulation of iNOS on Immune Cells and Its Role in Diseases. ***Int J Mol Sci.*** 19(12):3805 (2018).

73. Han Y., et al. PD-1/PD-L1 pathway: current researches in cancer. ***Am J Cancer Res.*** 10(3):727-742 (2020).

74. Chrabańska M., et al. Association between PD-L1 Expression and the Prognosis and Clinicopathologic Features of Non-Clear Cell Renal Cell Carcinoma. ***Int J Mol Sci.*** 25(7):3916 (2024).

75. Roy M., et al. The Role of Tumor Stroma in Cancer Progression and Prognosis: Emphasis on Carcinoma-Associated Fibroblasts and Non-small Cell Lung Cancer, ***Journal of Thoracic Oncology***. 6(1):209-217 (2011).

76. Kolesnikoff N., et al. Interrelationships between the extracellular matrix and the immune microenvironment that govern epithelial tumour progression. ***Clin Sci (Lond).*** 136 (5): 361-377 (2022).

77. Fotsitzoudis C., et al. Cancer-Associated Fibroblasts: The Origin, Biological Characteristics and Role in Cancer-A Glance on Colorectal Cancer. ***Cancers.*** 14(18):4394 (2022).

78. Roy M., et al. The Role of Tumor Stroma in Cancer Progression and Prognosis: Emphasis on Carcinoma-Associated Fibroblasts and Non-small Cell Lung Cancer, ***Journal of Thoracic Oncology***. 6(1):209-217 (2011).

79. Mao X., et al. Crosstalk between cancer-associated fibroblasts and immune cells in the tumor microenvironment: new findings and future perspectives. ***Mol Cancer*** 20:131 (2021).

80. Van Steensel B., et al. Partial colocalization of glucocorticoid and mineralocorticoid receptors in discrete compartment in nuclei of rat hippocampus neurons. ***J. Cell Sci.*** 109:787-792 (1996).

81. Klingberg F., et al. The myofibroblast matrix: implications for tissue repair and fibrosis. ***J Pathol.*** 229(2):298-309 (2013).

82. Hartsock A., Nelson WJ. Adherens and tight junctions: structure, function and connections to the actin cytoskeleton. ***Biochim Biophys Acta***. 1778(3):660-669 (2008).

83. Radvanyi L.G., et al. Specific lymphocyte subsets predict response to adoptive cell therapy using expanded autologous tumor-infiltrating lymphocytes in metastatic melanoma patients. ***Clin Cancer Res.*** 18(24):6758-6770 (2012).

84. Mannan A., et al. Advancing the frontiers of adaptive cell therapy: A transformative mechanistic journey from preclinical to clinical settings, ***Intl Immunopharmacol.*** 125, 567-5769 (2023).

85. Facciabene A., et al. T-regulatory cells: key players in tumor immune escape and angiogenesis. ***Cancer Res.*** 72(9):2162-2171 (2012).

86. Qiu Y., et al. FOXP3+ regulatory T cells and the immune escape in solid tumours***. Front Immunol.*** 13:982986 (2022).

87. Li C., et al. Regulatory T cells in tumor microenvironment: new mechanisms, potential therapeutic strategies and future prospects. ***Mol Cancer.*** 19:116 (2020).

88. Schürch C.M., et al. Coordinated Cellular Neighborhoods Orchestrate Antitumoral Immunity at the Colorectal Cancer Invasive Front. ***Cell.*** 182(5):1341-1359 (2020).

89. Certo M., et al. Endothelial cell and T-cell crosstalk: Targeting metabolism as a therapeutic approach in chronic inflammation. ***Br J Pharmacol.*** 178(10):2041-2059 (2021).

90. Wienke J., et al. T cell interaction with activated endothelial cells primes for tissue-residency. ***Front Immunol.*** 13:827786 (2022).

91. Ryan B.M., Faupel-Badger J.M. The hallmarks of premalignant conditions: a molecular basis for cancer prevention. ***Semin Oncol.*** 43(1):22-35 (2016).

92. Curtius K., et al. Evolution of Premalignant Disease. ***Cold Spring Harb Perspect Med***. 7(12):a026542 (2017).

93. Smith C.J., et al. Analysis of Tumor Biology to Advance Cancer Health Disparity Research. ***Am J Pathol.*** 188(2):304-316 (2018).

94. Chen F.W., et al. Advanced-Stage Colorectal Cancer in Persons Younger Than 50 Years Not Associated With Longer Duration of Symptoms or Time to Diagnosis. ***Clin Gastroenterol Hepatol.*** 15(5):728-737 (2017).

95. Que S.K.T. et al. Cutaneous squamous cell carcinoma: Management of advanced and high-stage tumors. ***J Am Acad Dermatol.*** 78(2):249-261 (2018).

96. Diederichsen A.C., et al. Prognostic value of the CD4+/CD8+ ratio of tumour infiltrating lymphocytes in colorectal cancer and HLA-DR expression on tumour cells. ***Cancer Immunol Immunother.*** 52(7):423-428 (2003).

97. Yang Y., et al. Crosstalk between hepatic tumor cells and macrophages via Wnt/β-catenin signaling promotes M2-like macrophage polarization and reinforces tumor malignant behaviors. ***Cell Death Dis*** 9:793 (2018).

98. Bielenberg D.R., Zetter B.R. The Contribution of Angiogenesis to the Process of Metastasis. ***Cancer J.*** 21(4):267-273 (2015).

99. Madu C.O., et al. Angiogenesis in Breast Cancer Progression, Diagnosis, and Treatment. ***J Cancer.*** 11(15):4474-4494 (2020).

100. Ngaha T.Y.S., et al. Angiogenesis in lung cancer: Understanding the roles of growth factors. ***Cancers.*** 15(18):4648 (2023).

101. Yao C., et al. Angiogenesis in hepatocellular carcinoma: mechanisms and anti-angiogenic therapies. ***Cancer Biol Med.*** 20(1):25-43 (2023).

102. Prakash J., Shaked Y. The Interplay between Extracellular Matrix Remodeling and Cancer Therapeutics. ***Cancer Discov***. 14(8):1375-1388 (2024).

103. Chen Y., et al. Clinical and therapeutic relevance of cancer-associated fibroblasts. ***Nat Rev Clin Oncol.*** 18(12):792-804 (2021).

104. Sahai E., et al. A framework for advancing our understanding of cancer-associated fibroblasts. ***Nat Rev Cancer*** 20:174-186 (2020).

Acknowledgements

This work is supported by NIH grants no. U2C CA233311 (M.P.S., J.M.F., C.C., W.J.G.), no. 1U54HG010426 (M.P.S., W.J.G.), no. RM1-HG007735, no. UM1-HG009442, no. UM1-HG009436, no. R01-HG00990901 and no. U19-AI057266 (to W.J.G.). Y. Lin of Washington University in St. Louis provided the B001, B004, B005 and B006 HuBMAP healthy colon tissue samples (for comparison with the FAP affected tissues). BioRender was used for generating Figs.1a and 2a.

Author contributions

T.K.G, M.P.S., J.M.F., and W.J.G. conceptualized the study. T.K.G. generated the histology slides, performed CODEX multiplexed imaging, analyzed the data and generated the figures. R.L., M.M., A.M.H., U.L., E.D.E., A.K.W., E.M., K.P., R.C., S.W., J.B. were responsible for sample collection. A.M.H., A.K.W. and E.M. were involved in project coordination. W.R.B. assisted in preparing the original CODEX panel. T.L. and J.S. performed histopathologic assessment of the samples. D.C. and T.K. handled data management and submission to repositories. T.K.G. and M.P.S. wrote the original draft of the manuscript. All authors reviewed and edited the manuscript. C.C., E.D.E., J.M.F., M.P.S. and W.J.G. were responsible for funding acquisition. M.P.S. and J.M.F. supervised the project.

Competing interests

MPS is a cofounder and scientific advisor of Crosshair Therapeutics, Exposomics, Filtricine, Fodsel, iollo, InVu Health, January AI, Marble Therapeutics, Mirvie, Next Thought AI, Orange Street Ventures, Personalis, Protos Biologics, Qbio, RTHM, SensOmics. MPS is a scientific advisor of Abbratech, Applied Cognition, Enovone, Jupiter Therapeutics, M3 Helium, Mitrix, Neuvivo, Onza, Sigil Biosciences, TranscribeGlass, WndrHLTH, Yuvan Research. MPS is a cofounder of NiMo Therapeutics. MPS is an investor and scientific advisor of R42 and Swaza. MPS is an investor in Repair Biotechnologies. W.J.G. is a consultant and equity holder for 10x Genomics, Guardant Health, Quantapore and Ultima Genomics, and cofounder of Protillion Biosciences, and is named on patents describing ATAC-seq. EDE is an employee and

stockholder of Labcorp Genetics and an advisor and stockholder of Taproot Health, Exir Bio, and ROMTech. The remaining authors declare no competing interests.

Fig. 1a.

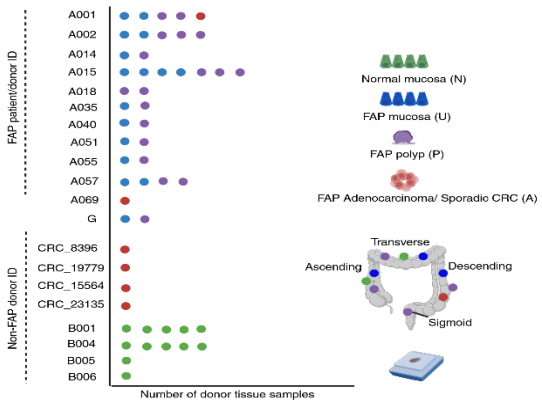

b.

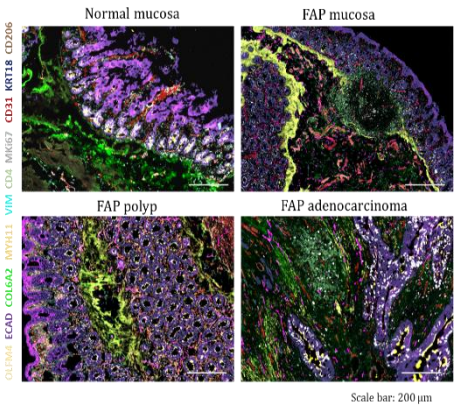

c.

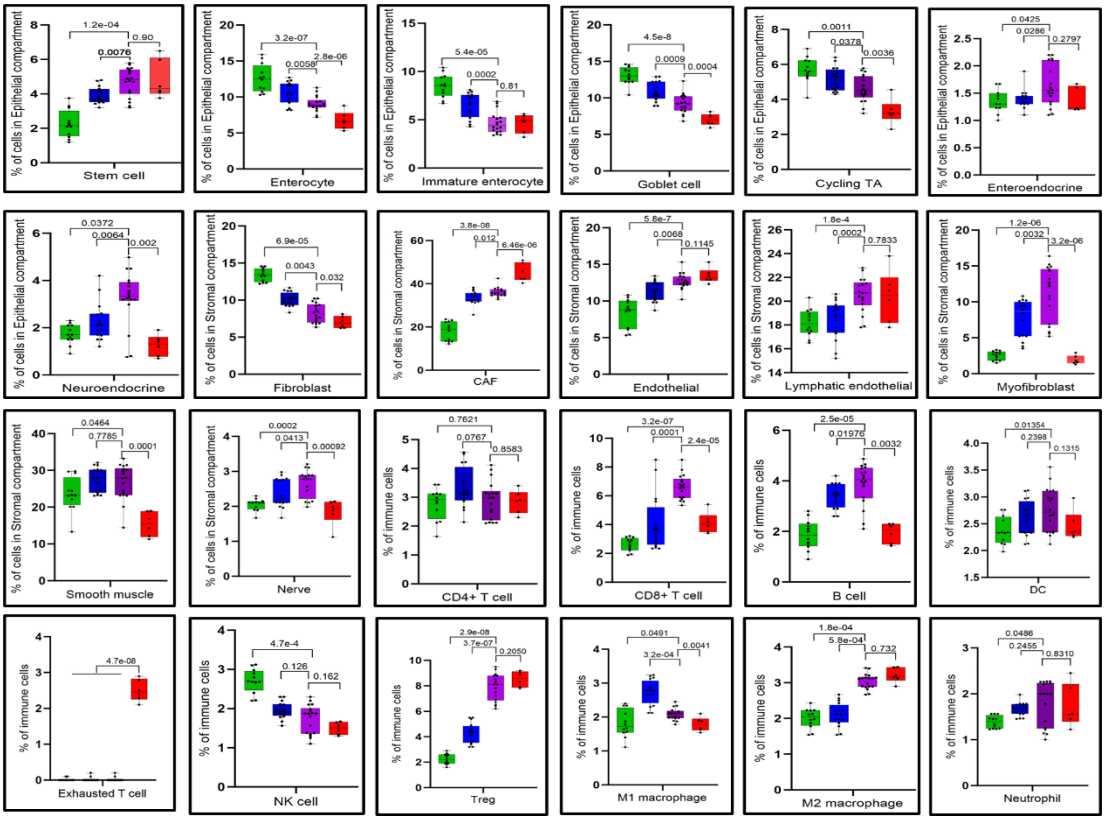

d.

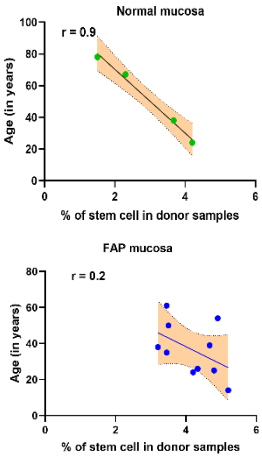

e.

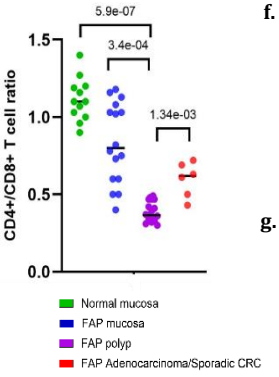

f.

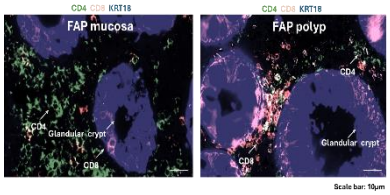

g.

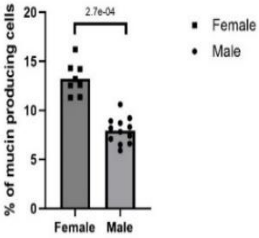

Fig. 1. Single-cell CODEX imaging of FAP tissue samples shows changes in cell type composition within colon microenvironment. **a**. shows the number of donor tissue samples from FAP and non-FAP patients, including the normal mucosa samples from HuBMAP samples as healthy controls. The tissue and polyp samples have been collected from different regions of the colon. Normal mucosa: green, FAP mucosa: blue, FAP polyp: magenta, and FAP adenocarcinoma/Sporadic CRC: red. The flash frozen samples have been embedded in Optimal cutting temperature (OCT) solution for sectioning at 8 μm and eventually used for single-cell imaging using Akoya's CODEX/Phenocycler platform. The pathological stages have been graded independently by two certified pathologists, **b.** shows representative CODEX images from normal mucosa, FAP mucosa, FAP polyp, and FAP adenocarcinoma/Sporadic CRC. The tissue sections have been stained with 40 barcoded antibodies and interrogated with corresponding florescent reporters in each imaging cycle (3 reporters/imaging cycle). For simplicity, 9 markers have been shown here. Scale bar: 200 μm, **c.** shows boxplots depicting the fraction of cell types in a given compartment (epithelial, stromal, immune). Each box represents data from a single disease state. Wilcoxon comparisons have been made to FAP polyps in each case. The stem cells, endothelial cells, cancer-associated fibroblasts (CAFs), regulatory T cells (Tregs), M2 macrophages increased while enterocytes, goblet cells, cycling TA, Natural-killer cells (NK) decreased along the disease continuum, **d.** Top panel shows strong correlation (Pearsson coefficient, r= 0.9) between percentage of stem cell population with age from four healthy individuals, where the stem cell population decrease with increase in age. Bottom panel: shows no correlation (Pearson coefficient, r= 0.2) between percentage of stem cell population with age from FAP individuals, ruling out the possibility of decrease in stem cell population as a result of aging, **e.** depicts the ratio of CD4+ and CD8+ T cells across the disease continuum. Higher CD4+ T: CD8+ T cell ratio (above 1) corresponds to increased immune function, as expected in normal mucosa. This ratio declines (below 1) during the disease progression suggesting decreased CD4+ T cell levels and increased activity of cytotoxic CD8+ T cells within the precancer microenvironment. Statistical comparison has been made between FAP polyps and other disease states/normal mucosa, **f.** Representative image showing CD4+ T cell population higher in FAP mucosa compared to that of FAP polyp. Alternatively, CD8+ T cell population within FAP polyp increases compared to the FAP mucosa counterpart and these cytotoxic T cells have been shown to be spatially located near the glandular crypts, **g.** Bar graph showing higher percentage of mucin-producing goblet cells lining the colon epithelial layer within female patients compared to male patients, which is statistically significant.

Fig. 2a.

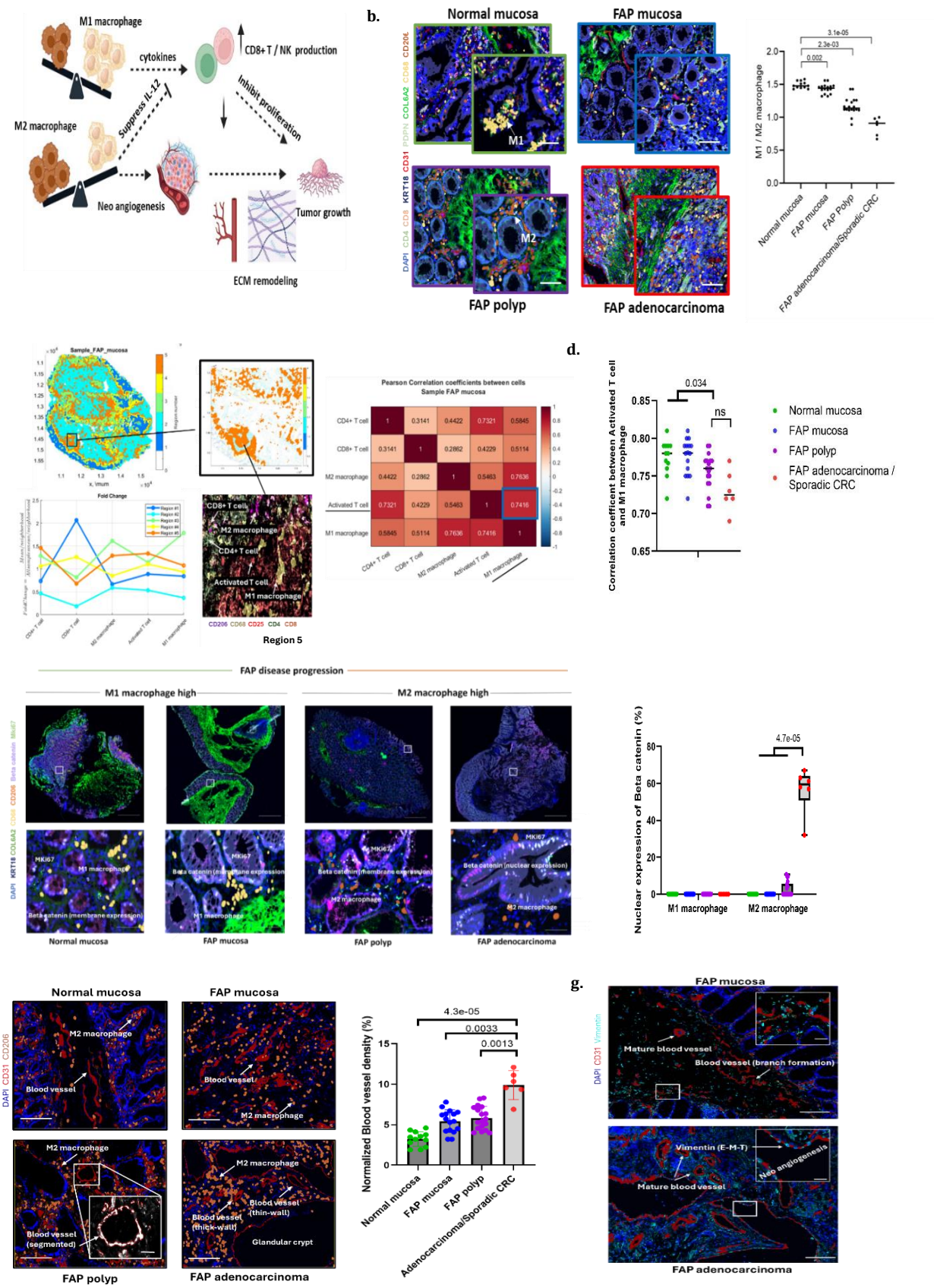
M1 macrophage
cytokines
CD8+ T / NK production
Suppress IL-12
Inhibit proliferation
M2 macrophage
Neo angiogenesis
Tumor growth
ECM remodeling
b.
Normal mucosa
FAP mucosa
FAP polyp
FAP adenocarcinoma
M1
M2
M1 / M2 macrophage
Normal mucosa
FAP mucosa
FAP Polyp
FAP adenocarcinoma/Sporadic CRC
c.
Region 5
CD8+ T cell
M2 macrophage
CD4+ T cell
Activated T cell
M1 macrophage
Pearson Correlation coefficients between cells
Sample FAP mucosa
d.
Correlation coefficient between Activated T cell and M1 macrophage
0.034
ns
Normal mucosa
FAP mucosa
FAP polyp
FAP adenocarcinoma / Sporadic CRC
e.
FAP disease progression
M1 macrophage high
M2 macrophage high
Normal mucosa
FAP mucosa
FAP polyp
FAP adenocarcinoma
Nuclear expression of Beta catenin (%)
4.7e-05
M1 macrophage
M2 macrophage
f.
Normal mucosa
FAP mucosa
M2 macrophage
Blood vessel
Blood vessel (segmented)
Blood vessel (thick-wall)
Blood vessel (thin-wall)
Glandular crypt
FAP polyp
FAP adenocarcinoma
Normalized Blood vessel density (%)
4.3e-05
0.0033
0.0013
Normal mucosa
FAP mucosa
FAP polyp
Adenocarcinoma/Sporadic CRC
g.
FAP mucosa
Mature blood vessel
Blood vessel (branch formation)
Vimentin (E-M-T)
Neo angiogenesis
Mature blood vessel
FAP adenocarcinoma

Fig. 2. Effect of M1 and M2 macrophages during FAP disease progression. **a.** This figure shows the importance of M1 and M2 macrophage ratio and its role in tumor progression. When M1 macrophage is higher, M1 macrophage secretes immunostimulatory cytokines which activate CD8+ T cells and NK cells, which impedes cancer cells growth. However, when M2 macrophage population is higher, tumor-associated antigens suppress interleukin 12, which hinders CD8+ T cell production thereby helping tumor proliferation. Higher M2 macrophage also modulates tumor microenvironment via neo-angiogenesis and extracellular matrix remodeling. **b.** Representative images of M1 and M2 macrophage as seen in normal mucosa, FAP mucosa, FAP polyp and FAP adenocarcinoma. M1 macrophage is anti-tumorigenic while M2 macrophage is pro-tumorigenic leading to malignancy. We find higher M1/M2 macrophage ratio (statistically significant) in normal mucosa when compared to that of FAP diseased states, **c.** Top panel (left): Spatial map of a representative FAP mucosa sample showing the colocalization of M1 macrophage with activated T cells within region 5 (marked with orange) of the sample, which is expected, as M1 macrophage activates/primes CD4+ helper T cells. Bottom panel (left): A graph showing fold change of selective immune markers, specifically T cells within each region indicating the localization of activated T cells and other T cell population with respect to M1 and M2 macrophage. Heatmap showing highest Pearson correlation coefficient between activated T cell and M1 macrophage (r=0.7461) when compared to CD4+ T (r=0.584) and CD8+ T cell (r=0.5114), **d.** Graph showing correlation coefficient between activated T cell and M1 macrophage across the tissue samples and diseased states showing activated T cells and M1 macrophages have statistically significantly higher correlation coefficient values within normal mucosa and FAP mucosa when compared to that of FAP polyp and FAP adenocarcinoma/sporadic CRCs, **e.** Representative CODEX images showing nuclear expression of beta-catenin within FAP adenocarcinoma/sporadic CRC samples, where M2 macrophage population has been found higher compared to the normal and FAP mucosa samples. Beta-catenin accumulation in nucleus results in transcriptional activation of target genes participating in malignant transformation. MKi67 marker has been included for representing nuclear expression. Graph showing significantly higher percentage for nuclear expression of Beta-catenin within FAP adenocarcinoma/sporadic CRC samples in the presence of M2 macrophage, **f.** Representative CODEX images showing blood vessels (red, segmented represented with white color) in the presence of M2 macrophage (orange) within normal, FAP mucosa, FAP polyp and adenocarcinoma. Thin-walled and thick-walled blood vessels have been indicated within the FAP adenocarcinoma sample. Bar graph showing normalized blood vessel density (%) across the tissue samples, showing significantly higher percentage of blood vessel density within adenocarcinoma/CRC samples, **g.** Top panel: CODEX image showing mature blood vessel and blood vessel with branch formation or microstructures within FAP mucosa, Bottom panel: FAP adenocarcinoma showing mature blood vessels along with formation of new blood vessels through a process known as neo-angiogenesis (inset). Tumor cells require a higher supply of nutrition and oxygen for proliferation. Vimentin is a marker for Epithelial-to-Mesenchymal transition, which is also expressed on the endothelial lining during neo-angiogenesis.

Fig. 3a.

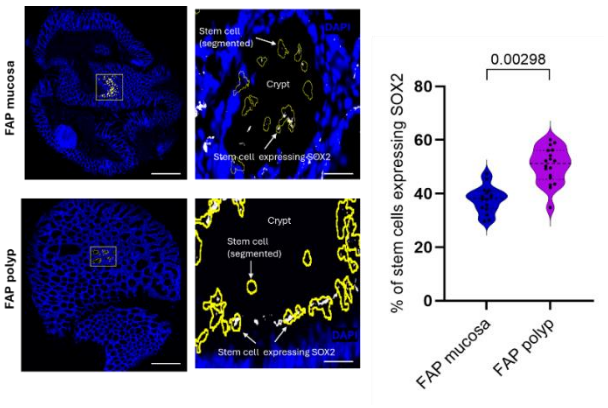

b.

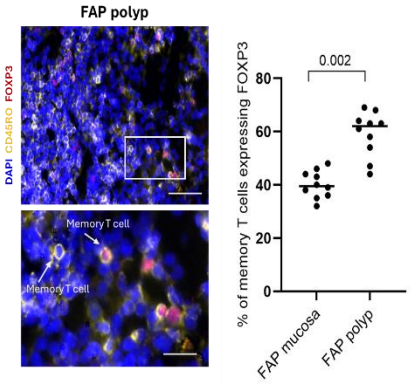

c.

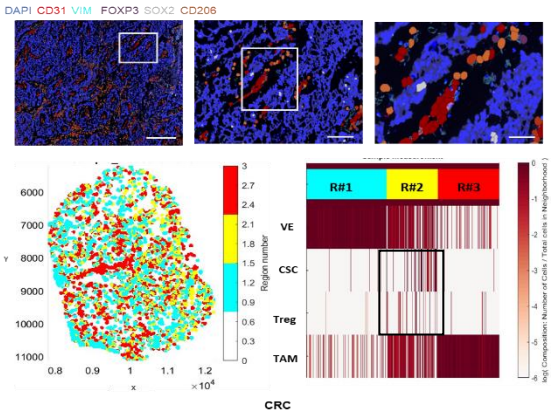

d.

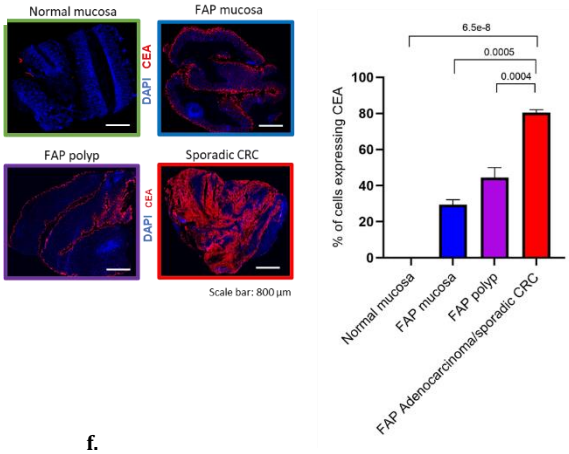

e.

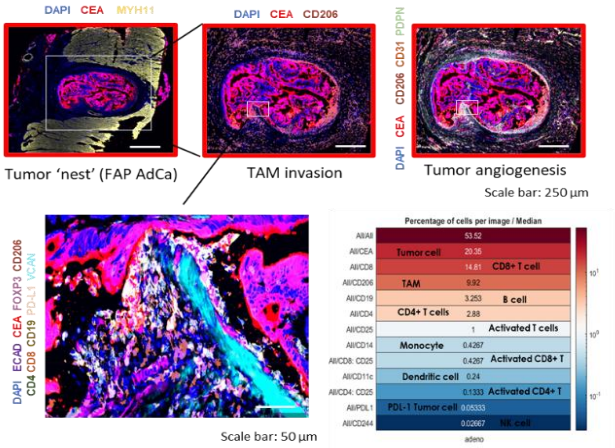

f.

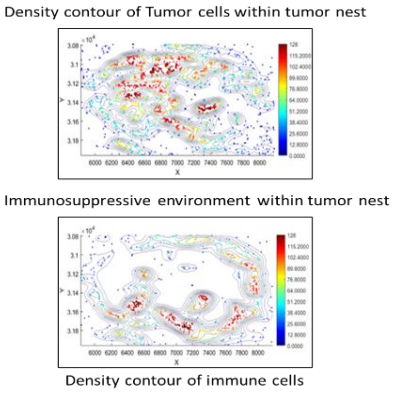

g.

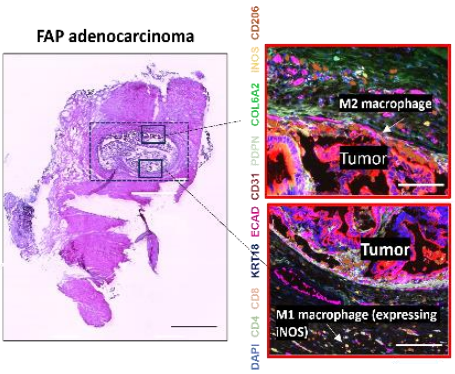

h.

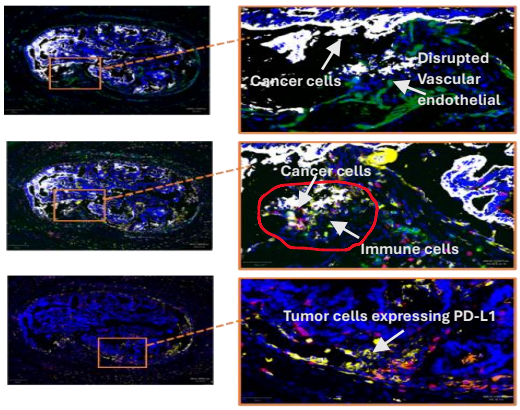

Fig. 3. Dynamic interaction of cancer cells and immune cells within FAP adenocarcinoma/sporadic CRC microenvironment. a. Representative CODEX images of FAP mucosa and FAP polyp samples showing fraction of stem cells that are expressing cancer stem cell marker, SOX2. FAP polyps have a statistically significant higher percentage of stem cells expressing SOX2 than that of FAP mucosa., **b.** shows FAP polyps have higher percentage of memory T cells expressing FOXP2 (statistically significant), thereby transforming into higher number of regulatory T cells when compared with FAP mucosa, **c.** Regulatory T cells (Tregs) are situated near cancer stem cells which are in the intestinal glandular crypts. It has been shown that Tregs help in cancer stem cell proliferation by secreting TGF-β, interleukins int tumor microenvironment, and also control CSCs via angiogenesis and through indirect tumor associated macrophage (TAM) effect, **d.** CODEX images showing increased expression of carcinoembryonic antigen (CEA) during the FAP disease progression and bar plot shows the quantification. As expected, FAP adenocarcinoma and sporadic CRCs express significantly higher than the other diseased state while normal mucosa don't express CEA, **e.** CEA marker has been useful to image the tumor 'nest' in one FAP adenocarcinoma sample. Cancer cells recruit TAMs near its periphery which results in tumor angiogenesis. Several immune cells such as CD4+ T, CD8+ T, B cells have been found in the 'nest' boundary. A typical composition of tumor microenvironment has been presented, **f.** Density contour of cancer cells within the tumor 'nest' (upper panel), density contour of immune cells near the tumor boundary and absent from the tumor 'nest' depicting an immunosuppressive tumor microenvironment, **g.** Codex image showing the presence of TAMs at tumor invasive front, while M1 macrophages have been shown further away from the tumor. M1 macrophages express inducible nitric oxide synthase as a part of macrophage inflammatory/adaptive response, **h.** Codex images showing the escape of cancer cells (white) from the tumor nest by disrupting the vascular endothelial cells (green). Near the escape point, a bunch of immune cells comprising of CD8+ T cell, CD4+ T cell, B cell counteracts with the invading cancer cells, thereby preventing the tumor progression.

Fig. 4a.

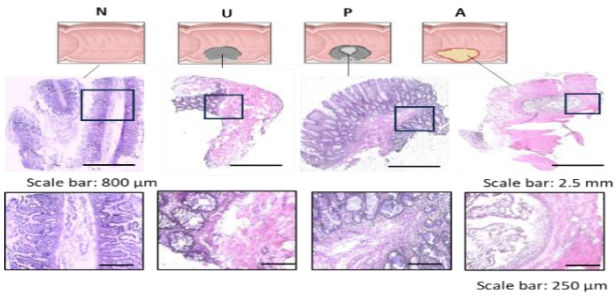

b.

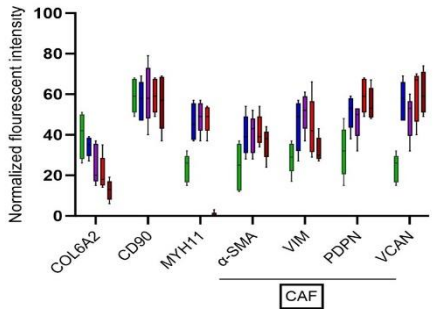

c.

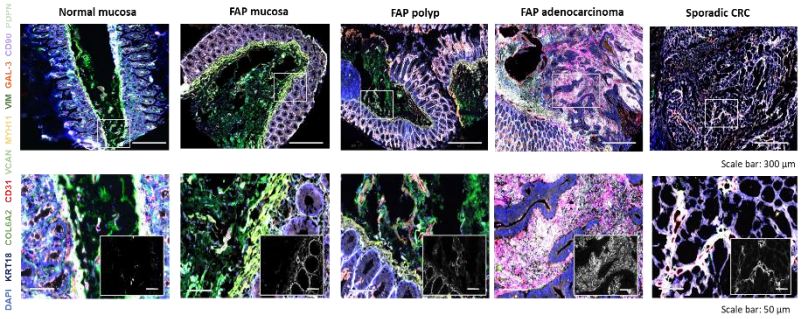

d.

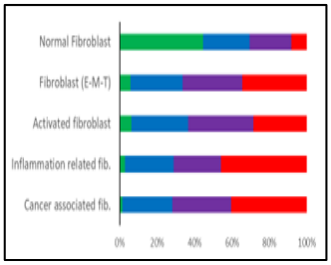

e.

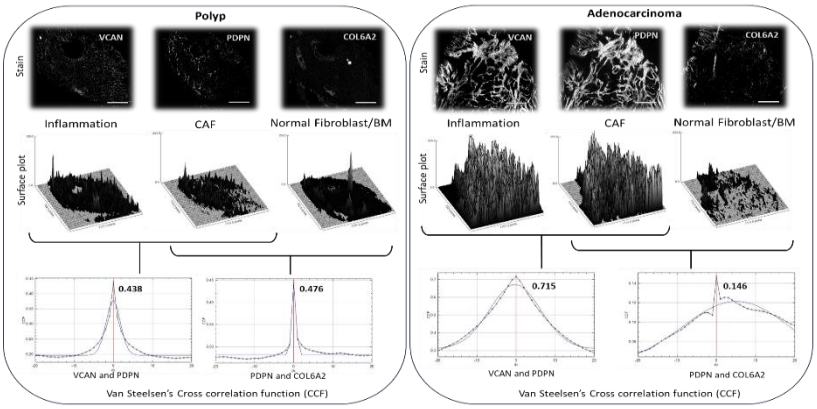

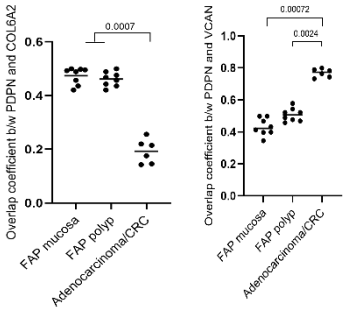

f.

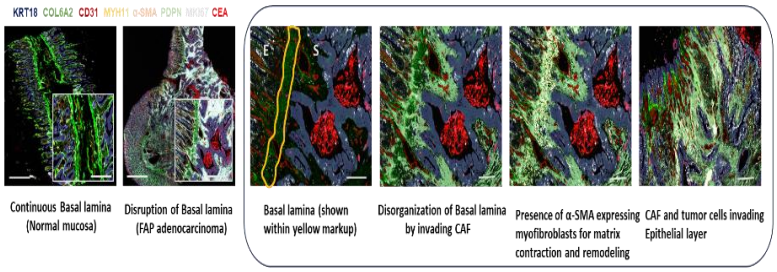

g.

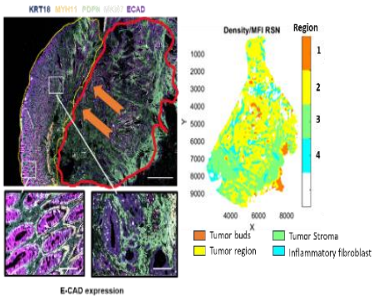

h.

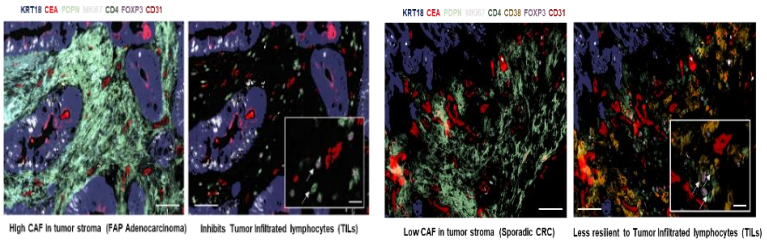

i.

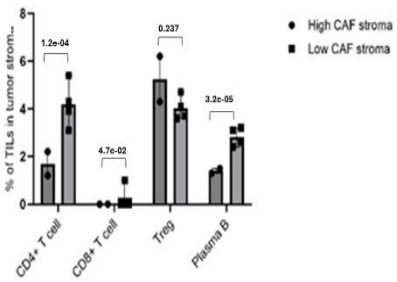

Fig. 4. Role of Cancer associated fibroblasts (CAFs) in FAP disease progression. a. This figure shows representative H&E images of stromal compartments from normal mucosa samples and other FAP diseased states. The images within the box have been magnified, **b.** shows normalized fluorescent intensity of various stromal markers including CAFs such as alpha-SMA, Vimentin, Podoplanin and Versican. As expected, collagen expression is higher in normal mucosa while lower in the rest of the FAP diseased tissue samples, **c.** shows the CODEX images of stromal compartment imaged with the stromal markers. The inset shows a CAF marker expression (Podoplanin), which is absent from normal mucosa, **d.** shows % of normal fibroblast, fibroblast (EMT), activated fibroblast, inflammatory related fibroblast and cancer associated fibroblast. Except normal fibroblasts, all other fibroblasts are higher in the FAP disease continuum, **e.** this figure depicts the overlap between the inflammatory region and cancer associated fibroblasts (CAFs). VCAN = inflammatory marker, PDPN = CAF marker, COL6A2 = normal fibroblast/basal lamina. When both polyps and adenocarcinoma were stained with these markers, a surface plot of pixel intensity was generated using Image J software. The images were subjected to Van steelsen's cross correlation coefficient, which shows how the Pearson coefficient changes after shifting the red image voxel over the green image voxel. By observing the shape of CCF plot as a function of this shift, it can be determined if the signals of the two channels are actually positively correlated. The CCF between inflammatory marker (VCAN) and CAF marker (PDPN) increases within FAP adenocarcinoma sample, **f.** shows the graph with CCF values, where overlap CCF between PDPN and VCAN increase in adenocarcinoma/sporadic CRC while overlap CCF between PDPN and COL6A2 decreases in AdCa/CRC. This indicates that CAFs are present near inflammatory regions of the tissue and promote malignancy, **g.** CODEX images showing how CAFs (green) from stromal compartment invade colon epithelial layer by disorganizing the basal lamina. Expression of alpha-SMA on myofibroblasts further helps in matrix contraction and remodeling, **h.** E-Cadherin is required for cell-cell adhesion in normal/healthy mucosa. In adenocarcinoma, CAFs have been shown to suppress E-Cad expression (magenta) near its vicinity. This leads to weakening of cell-cell adhesion leading to tumor proliferation and metastases. On the other hand, E-cad expression is higher within epithelial compartments which are further away from CAFs migratory path, resulting in tight cell-cell adhesion (normal morphology). Spatial map of a tumor stroma has been shown to locate tumor region, tumor bud, and inflammatory fibroblasts, **i.** CODEX images showing how higher CAF population within stroma of FAP adenocarcinoma inhibits tumor infiltrated lymphocytes, thereby assisting in immunosuppressive microenvironment. TILs are a group of mononuclear T cells infiltrated from tumor tissue found in most solid tumors. TILs are found in stroma within tumor area and contain mostly T cells, and few B cells. Alternatively, lower CAF population within sporadic CRC inhibits TILs to a lesser extent, suggesting that CAFs are also responsible for dampening the effect of immune cells needed for eradicating the tumor cells, **j.** graph showing % of TILs in tumor stroma in the presence of either high or low CAF. In the presence of high CAF population in the tumor stroma, CD4+ T, CD8+ T and plasma B cells are decreased, while low CAFs promote statistically higher presence of these immune cells in their stromal microenvironment. It's interesting to see that regulatory T cells (Tregs) are not affected by either high or low CAFs. This results in a higher number of Tregs in the tumor environment.

Fig. 5a.

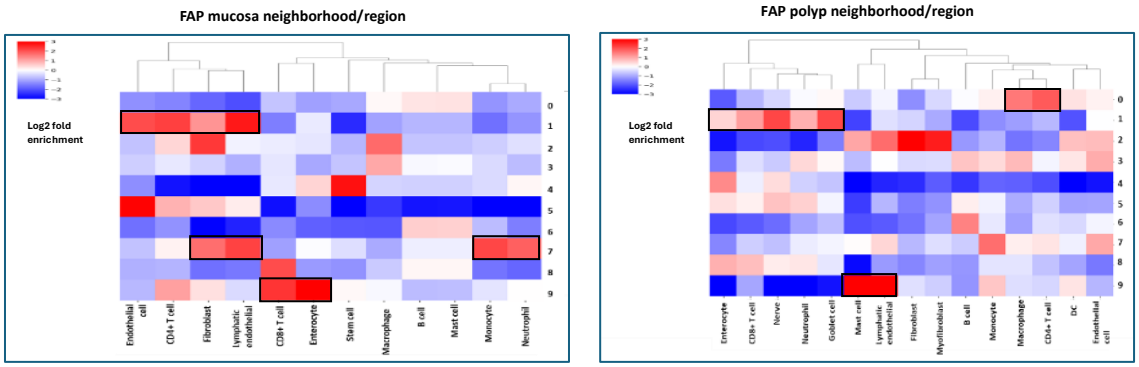
FAP mucosa neighborhood/region
Log2 fold enrichment
Endothelial cell
CD4+ T cell
Fibroblast
Lymphatic endothelial
CD8+ T cell
Enterocyte
Stem cell
Macrophage
B cell
Mast cell
Monocyte
Neutrophil
FAP polyp neighborhood/region
Log2 fold enrichment
Enterocyte
CD8+ T cell
Nerve
Neutrophil
Goblet cell
Mast cell
Lymphatic endothelial
Fibroblast
Myofibroblast
B cell
Monocyte
Macrophage
CD4+ T cell
DC
Endothelial cell

b.

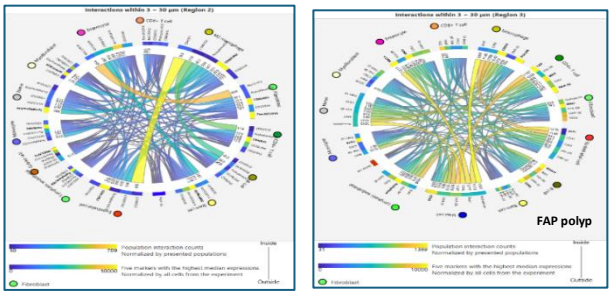
FAP polyp

c.

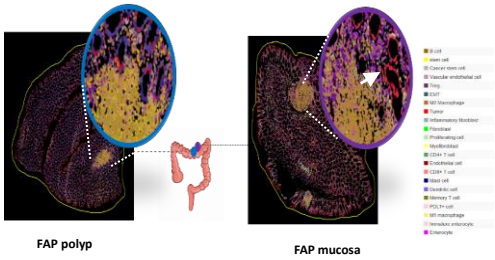
FAP polyp
FAP mucosa

d.

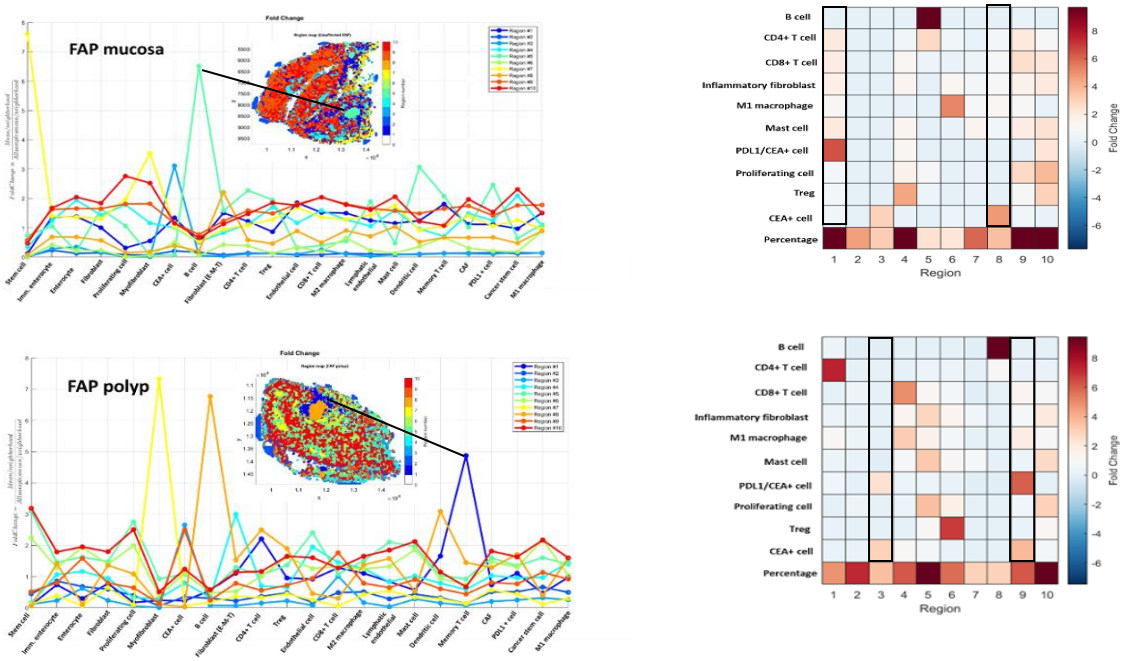
FAP mucosa
Fold Change
B cell
CD4+ T cell
CD8+ T cell
Inflammatory fibroblast
M1 macrophage
Mast cell
PDL1/CEA+ cell
Proliferating cell
Treg
CEA+ cell
Percentage
Region
FAP polyp
Fold Change

e.

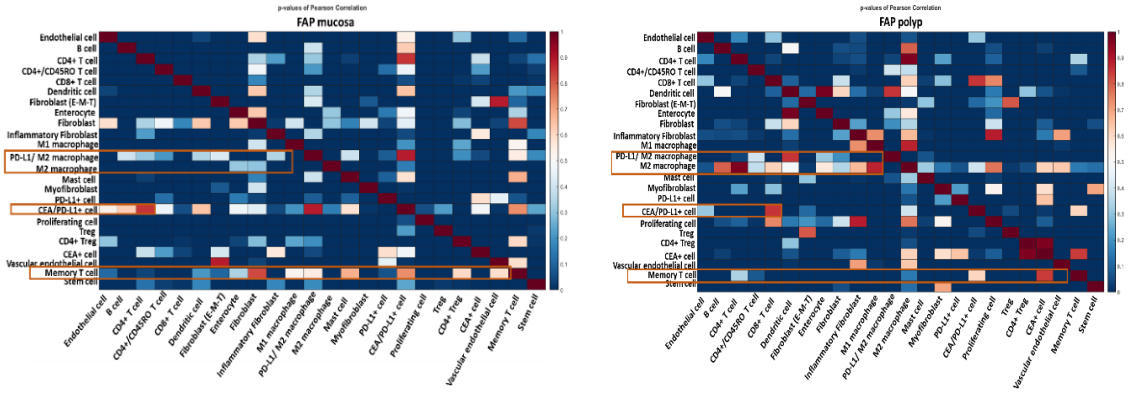
p-values of Pearson Correlation
FAP mucosa
Endothelial cell
B cell
CD4+ T cell
CD4+/CD45RO T cell
CD8+ T cell
Dendritic cell
Fibroblast (E-M-T)
Enterocyte
Fibroblast
Inflammatory Fibroblast
M1 macrophage
PD-L1/ M2 macrophage
M2 macrophage
Mast cell
Myofibroblast
PD-L1+ cell
CEA/PD-L1+ cell
Proliferating cell
Treg
CD4+ Treg
CEA+ cell
Vascular endothelial cell
Memory T cell
Stem cell
FAP polyp

Fig. 5. Neighborhood analyses between adjacent FAP mucosa and FAP polyp show differences in cell type location based on functionality. a. Heatmap showing the fold change of cell types in different regions from FAP mucosa samples (left) and FAP polyp samples (right). In both the cases, certain cell types colocalize within the same region because of functional/biological significance (marked with black outline). For example, in FAP mucosa, the endothelial cells (ECs) and CD4+ T cells reside within region 1, EC-T cell interactions control of T cell recruitment and activation. Similarly, monocytes and neutrophils migrate with lymphatic endothelial cells (region 7) while CD8+ T cells are found near the enterocytes, gaurding these epithelial cells from invading pathogens (region 9). In FAP polyp samples, macrophages and CD4+ T cells colocalize within region 0, which basically activates each other and prepare themselves for attacking any invading pathogens. Neutrophils migrate towards the intraepithelial zone and join CD8+ T cells (IELs) to further bolster the immune attack (region 1). Moreover, mast cells colocalize with lymphatic endothelial cells and migrate to different regions of the polyp tissue, **b.** Circos representation of cell-cell interaction within FAP mucosa and FAP polyp samples. Interactions between the cell types increase with the FAP disease progression (see text for details), **c.** Magnified image showing the precancer microenvironment near the lymphoid follicles found within adjacent FAP mucosa (blue) and FAP polyp (magenta). Epithelial cells expressing CEA+ marker within FAP polyp microenvironment is shown with white arrow, **d.** Line plots depicting fold change of different cell types from FAP mucosa (upper panel) and FAP polyp samples (lower panel). For example, B cell inside the lymphoid follcile (in FAP mucosa) and memory T cells outside the lymphoid follicle (in FAP polyp) has been indicated to their respective line plots. Overall, 10 regions were detected in both FAP mucosa and FAP polyp samples using neighborhood analyses. In FAP mucosa, where the severity of the cancer cells expressing PD-L1+/CEA+ tumor markers is low, we see immune cells within the same region as that of the tumor cells. Unlike FAP mucosa microenvironment, an immunosuppressive microenvironment is created where the PD-L1+/CEA+ expressing cells and immune cells segregate to separate regions, **e.** Heatmap showing the p-values of Pearson correlation coefficient for cell-cell interaction based on location within the adjacent FAP polyp samples. Several interesting differences in terms of cell-cell localization were found in FAP polyps when compared to that of FAP mucosa samples (see text for details)